Applied Thermal Engineering 300 (2026) 131334

Contents lists available at ScienceDirect

Applied Thermal Engineering

journal homepage: www.elsevier.com/locate/apthermeng

Research Paper

Operative envelope and boundary conditions of a small scale air-cooled power cycle with CO_2 mixtures at constant inventory

Matyáš Junek, Ettore Morosini *, Marco Astolfi, Giampaolo Manzolini

Politecnico di Milano, Dipartimento di Energia, Via Lambruschini 4, Milano, 20156, Italy

ARTICLE INFO

Keywords:
Cycle off-design
Transcritical CO2-mixtures
Settle out pressure
Air-cooled condenser
Constant inventory cycle

ABSTRACT

This work focuses on the definition of the operative envelope and the boundary conditions of a CO_2-blended transcritical power cycle in hot climate locations. This study is developed in the framework of the H2020 DESOLINATION project, focusing on understanding the potential of CO_2-blended power cycles for high temperature applications, particularly by investigating and predicting the off-design conditions of an innovative power cycle (i.e. a 1.8 MW_{el} air-cooled cycle operating at fixed inventory) designed within the project: some advanced features are included, such as the adoption of CO_2 + SO_2 mixture as working fluid, allowing for fluid condensation, and the use of unconventionally compact heat exchanger geometries. The power plant is designed through substantial interactions between the industrial partners involved, providing specifications of each component. Then, the operative envelope of the system is computed, presenting off-design cycle simulations at fixed inventory under variable ambient temperature and decreasing thermal input. Operative constraints that may limit the cycle operability in certain conditions are addressed acting on the air speed of the condenser. Results show that the constant inventory system could be operated in a wide range of conditions with absolute penalization in cycle efficiency up to 4% when compared to the design conditions (30% efficiency), aiming to guide development and the control strategy definition for a new category of CO_2-blended power plants. Finally, the equilibrium pressure in case of instantaneous plant shutdown (Settle Out Pressure) is computed with two different modeling approaches, helping in estimating the amount of fluid to be removed from the loop to safely operate the system during shutdowns or unpredicted operations.

1. Introduction and scope of work

Power cycles with supercritical CO_2 (sCO_2) as a working fluid have been studied by the scientific community over the last decades [1], pointing to high efficiencies, along with capital cost reductions, with respect to conventional cycles [2]. In particular, the performance attainable with sCO_2 cycles becomes competitive for maximum temperatures above 500 °C, leading to a reduction of the plant footprint and the overall system complexity with respect to conventional steam cycles [3]. While the interest in this research topic started decades ago with the first studies of Angelino [4] first and Dostal [5] more recently, many authors have contributed in the sCO_2 field by exploring the benefits of the technology for various applications such as nuclear [6], waste heat recovery [7], coal-fired power plants [8], concentrated solar power plants (CSP) [9]. Moreover, in the last few years, high temperature sCO_2 cycles have also been studied as heat pumps for pumped thermal energy storage systems [10], both in stand-alone configurations and in thermally-integrated ones. Those theoretical investigations led to the development of various sCO_2 cycle demonstrators, with the most prominent example being the STEP project, a US-funded project focused on a 10 MW_{el} sCO_2 recompression cycle [11].

At the same time other researchers, in particular from Europe, explored the possibility of operating a transcritical cycle with CO_2 mixtures aiming at an increase of the working fluid critical temperature and allowing for fluid condensation also in hot climate locations, in locations with a non-negligible share of operating hours during summertime at ambient temperatures above 35 °C: improvements of plants efficiency have been demonstrated, such as in CSP applications which are usually the ones mostly affected by performance penalization due to hot ambient temperatures and where easy access to water as coolant for the cycle heat rejection unit is not possible. Specifically, the main reason to prefer transcritical cycles with CO_2 mixtures as working fluid rather than pure sCO_2 cycles is related to the large drop in cycle efficiency of the latter ones when the cycle minimum temperature is above 45 °C [12] (typical for air-cooled applications in hot climates), where the sCO_2

* Corresponding author.
E-mail address: ettore.morosini@polimi.it (E. Morosini).

https://doi.org/10.1016/j.applthermaleng.2026.131334
Received 21 November 2025; Received in revised form 5 March 2026; Accepted 3 May 2026
Available online 4 May 2026

Nomenclature

Acronyms

CFD	Computational Fluid Dynamics
CSP	Concentrated Solar Power
HX	Heat Exchanger
HTC	Heat Transfer Coefficient
HTF	Heat Transfer Fluid
PCHE	Printed Circuit Heat Exchanger
PHE	Primary Heat Exchanger
sCO_2	Supercritical Carbon Dioxide
SOP	Settle Out Pressure
TES	Thermal Energy Storage
TIT	Turbine Inlet Temperature

Symbols

P	Pressure [bar]
ΔP	Pressure drop [bar]
T	Temperature [°C]
ΔT	Temperature difference [°C]
s	Specific Entropy [kJ/kg/K]
Nu	Nusselt Number
Re	Reynolds Number.
Pr	Prandtl Number
d_{hyd}	Hydraulic Diameter [m]
k	Thermal conductivity [W/m/K]
$f^{HTC,CFD}_{Correction,Mixture}$	Correction factor of the HTC on the mixture
$HTC^{1D-Straight}_{Convective}$	Convective HTC of the surrogate 1-D straight channel model [W/m^2/K]
$HTC^{Gyroidal}_{Convective}$	Convective HTC of the gyroidal PCHE computed in CFD [W/m^2/K]
$\dot{m}_{WF}$	Mass flow rate of the working fluid [kg/s]
ΔP_{SUB}	Subcooling pressure head [bar]
V_{air}	Air Volumetric flow rate [m^3/s]
$\dot{Q}_{IN}$	Thermal Input to the Cycle [MW]
η_{iso}	Isentropic Efficiency [−]
x_6	Vapor Quality of the Mixture at the Inlet of the Condenser [−]

compression, having an inlet condition far from the critical point, cannot benefit by fluid real gas effects. In alternative to transcritical cycle configurations, studies also demonstrated the benefit in using CO_2 mixtures with more volatile dopants in supercritical configuration keeping high compressor inlet temperatures above 50 °C [13]. Calculations show a remarkable improvement in efficiency with respect to sCO_2 cycles with same minimum and maximum temperatures enabling CO_2 mixture cycle to reach the same efficiency as sCO_2 cycle but adopting a much simpler architecture (i.e. simple recuperative cycle vs recompressed or partial cooling architectures).

The EU H2020 project SCARABEUS [14] developed specific methodologies for the identification of the most suitable mixtures mainly in CSP applications by adopting detailed cycle simulations [15,16] and extensive experimental activities on fluids compatibility, thermal stability and properties. As final stage of the project, a transcritical pilot loop with $CO_2 + C_6F_6$ mixture was operated in TU-Wien for hundreds of hours, proving the fluid thermal stability and the lack of operating issues for two different mixture compositions in a wide range of mass flow rates [17]. In last years some other mixtures, such as $CO_2 + SO_2$ or $CO_2 + TiCl_4$, were identified as promising blends able to provide net improvements in electric cycle efficiency with respect to pure sCO_2 cycles at constant boundary conditions by up to 2 percentage points (being around 4% relative gain in electrical power produced) [18], allowing to overcome the threshold of 50% cycle efficiency for next generation CSP plants at 700 °C while adopting minimum temperatures above 50 °C. Among the investigated mixtures, some of them such as $CO_2 + SiCl_4$ and the abovementioned $CO_2 + C_6F_6$ were also characterized from an experimental point of view with vapor-liquid equilibrium (VLE) analysis [19], bubble points and density measurements [20], pointing to promising efficiencies in CSP cycle configurations, overcoming the corresponding sCO_2 cycle efficiency at the same boundary conditions. Finally, annual analyses of CSP plants with CO_2-blended power plants demonstrate that this innovative solution could lead to a non-negligible LCOE reduction with respect to more conventional systems [21], while ensuring higher flexibility and higher efficiency than a sCO_2 cycle, especially at very low ambient temperatures (below 15 °C), where the sCO_2 cycle cannot benefit from a further reduction in minimum temperature.

To follow up on these studies and to improve the understanding of these innovative systems, in the EU H2020 project DESOLINATION the design and detailed study of a small CO_2-mixture power plant (about 1.8 MW_{el}) is carried out by both academic and relevant industrial partners, with the ambition to pave the path towards the construction and operation of a similar and analogous system in real CSP applications [23]. The $CO_2 + SO_2$ mixture (82% molar in CO_2) was identified as the most promising working fluid for this application, optimizing the composition with the aim of maximizing the cycle efficiency. The main advantages in using sulfur dioxide as dopant are related to (i) good thermal stability (tested up to 550 °C in static and cyclic tests) [22], (ii) high compatibility with materials and metals tested through extensive experimental campaign, (iii) favorable thermodynamic properties when mixed with CO_2 (e.g. proper impact on critical temperature increase) and (iv) relevant increase of performance with respect to pure sCO_2 cycle [23,24].

At the same time, concerns related to the toxicity of SO_2 have been dealt with by the project partners of DESOLINATION project in multiple ways: (i) at first, a detailed design of the turbine and pump dry gas seals was carried out, aiming at the minimization of the fluid leakages, (ii) then, a proper sizing of all the equipment required to recover and recirculate the leaks is accurately done, (iii) the definition and adoption of a wet scrubber has been foreseen for the final desulphurization of the remaining unavoidable leaks; finally (iv) a vent dispersion analysis has been carried out to evaluate SO_2 emissions distribution of the working fluid vent (e.g. after a fail in the emergency shut down procedure) ensuring that the surrounding regions will be interested by SO_2 concentrations way below the limit for avoiding dangers for life and health and assuming an instantaneous evacuation of the personnel from the plant (i.e. 100 ppm defined as the immediately dangerous to life or health). Additional investigations to mitigate the risks related to sulfur dioxide, such as the design of ventilation systems in the buildings, are considered out of the scope of this work.

Moreover, sulfur dioxide has been preferred to different dopants such as hydrocarbons, fluorocarbons and siloxanes for its good thermal stability, even if multiple literature works have suggested their use [25,26], since these categories of dopant cannot guarantee temperatures above 400–450 °C. SO_2 also presents suitable characteristics that noble gases and lighter gases (such as He, Xenon, N_2, O_2, H_2S, SF_6) cannot have, even if already considered in literature for CO_2-mixtures, being unable to ensure the transcritical configuration of power cycle with a limited amount of dopant in the mixture [13,27,28].

The use of SO_2 as dopant also poses some uncertainties if the plant would be controlled with a variable inventory as commonly proposed in power plants operating in pure CO_2, where an external inventory management system continuously introduces/removes fluid mass to/from the loop depending on the operating conditions. This controlling

strategy is already adopted in the sCO_2 loop of the demo plant of the STEP project in US [29] and already considered in literature to ease the system transient behavior during startups and shutdowns [30]. A similar approach for the inventory management of small scale sCO_2 loops is to have two dedicated working fluid tanks, one for the high-pressure side and one for the low-pressure one, as in the Brunel University test loop [31]. A preliminary analysis of the transcritical CO_2 blended power plant of interest in this work has been proposed in literature by considering a variable inventory configuration [32], showing that it is possible to operate the system in a wide operating envelope, having an inventory management system that is able to remove up to 20% of the overall inventory in the loop. Differently, the use of a constant inventory system dramatically simplifies the management of the plant limiting the number of auxiliaries components (valves, tanks, etc) and leads to an increase of system reliability with a reduction of fluid leakages that is an aspect of particular relevance in case of use of SO_2 as dopant. However, only a very limited number of theoretical studies are available on the analysis of the off-design behavior of fixed inventory CO_2 based power plants, as for the work of Alfani on sCO_2 cycle in heat recovery applications [33]. On the other hand, according to the authors best knowledge, no study is available on the off-design operation of fixed-inventory transcritical cycles with CO_2 mixtures which has been identified as a significant literature gap to be filled with this work, detailing the condensation process and ensuring a constant subcooling degree at the pump inlet. The specific characteristics of components and plant behavior are hence related to a specific plant studied by the partners of the project, even though the analysis proposed in this work follows a methodology that can be reproposed for any other plant operating with any CO_2 dopant, and it is not strictly case-specific to the DESOLINATION project.

While focusing on the specific characteristics of the small scale cycle proposed and investigated on a theoretical level within the DESOLINATION project, the objective of this work is to provide results not available in literature today on two main aspects:

- To study the constant inventory off-design behavior of the selected transcritical blended CO_2 cycle in a wide operative envelope considering different loads (down to 50% in thermal input) and different ambient temperatures (down to −30 °C with respect to the design ambient temperature). The trend of main thermodynamic parameters resulting in off-design are discussed (temperature and pressures), as well as the performance of the turbomachinery with their specific operative maps and the cycle efficiency including also condenser auxiliary consumption. The analysis is first carried out at air cooled condenser fan nominal speed and then at optimized fan rotational speed introducing constraints suggested by industrial partners: (minimum subcooling at pump inlet, vapor phase at condenser inlet) as explained in detail in Section 4. The analysis of the constrained off-design behavior of the system is highly iterative and required the development of a dedicated numerical tool.
- To discuss methodologies for the approximate calculation of the Settle Out Pressure, namely the pressure that the system reaches in case of malfunctioning of the turbine, activation of the trip valve and opening of the bypass valve considering an instantaneous equilibration of pressures. The quantification of this parameter is generally not very relevant for a Rankine cycle, where a large amount of fluid in liquid state remains in the condenser, but it has been recognized as of paramount importance for supercritical cycles and transcritical cycles. In the conditions investigated in this work, the expected increase in the cycle minimum pressure can be relevant and can cause damage of the equipment on the low-pressure side of the system (i.e. condenser manifolds, recuperator, pump intake and turbine outlet sections) after an emergency shutdown requiring additional margin in the design of low pressure side equipment (i.e. air cooled condenser, recuperator hot side, piping and flanges of turbine and pump).

The paper is structured as follows: in Section 2, the authors recall the characteristics of small scale transcritical cycle defined within the DESOLINATION project, already available in literature [32]. In Section 3 the overall methodology for the off-design analysis of the cycle is described. Section 4 presents the results of the cycle conditions at variable ambient temperature and thermal input by imposing the air velocity on the fan of the air-cooled condenser at design value and highlighting operating conditions not respecting the operative constraints. Subsequently, results obtained by reducing the air flow rate at the condenser fan are discussed, fulfilling the different components requirements and optimize cycle efficiency. Finally, in Section 5 the authors introduce different methodologies to evaluate the plant settle out pressure.

2. Characteristics of the cycle and performances at design conditions

The schematization of the simple recuperative cycle is shown in Fig. 1. The main components are a pump, a countercurrent recuperator, a primary heat exchanger (PHE), a turbine and an air-cooled condenser adopted as heat rejection unit. According to the analysis carried out within the H2020 DESOLINATION project, the cycle can be coupled with a thermal desalination plant based on forward osmosis (from point 6 to 6′ in Fig. 1): nevertheless, considering the project perspective, only 5% of the thermal power of the condenser is expected to be recovered from the desalination plant and not continuously during power plant operation. Thus, the section is not modelled in this work as an actual heat exchanger, but only with the corresponding additional volume, without describing the characteristics and performance of the desalination section. To simulate the conditions of a real CSP plant, the system is operated with molten salts as heat transfer fluid (HTF) as hot source, heated through an electric heater, controlling the mass flow rate through a HTF pump. The heat rejection system operates with ambient air as cooling medium, with no water consumption, to be representative of an arid location typical of CSP plants. The working fluid inventory is not varied during cycle operation to have a simplified design and control strategy. The internal volumes of the cycle components are fully defined, and the overall inventory distributes into the internal volume of the loop according to actual operative condition, determining an additional constraint on plant operation and condition during shut-downs.

To briefly summarize the main design choices and sizing of the plant components, Table 1 reports the main assumptions regarding cycle thermodynamic design (temperature and pressures) and components performance and specifications, while Table 2 lists the power balance of each component at design and the relevant figures of merit of HXs [9]. The ambient temperature of 40 °C is set to represent the operation of the system in a hot location, while the cycle minimum temperature above 50 °C is necessary to ease the heat transfer capability of the condenser,

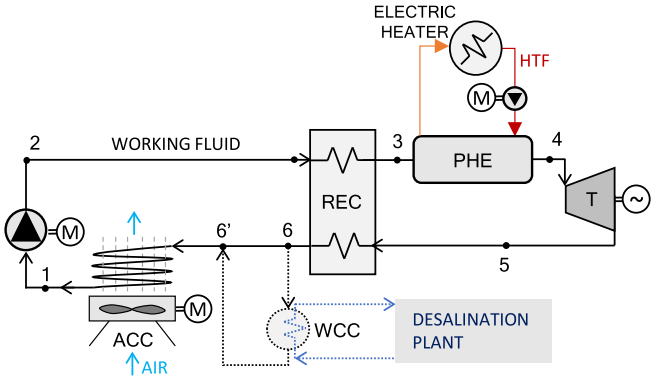

Fig. 1. Schematization of the foreseen DESOLINATION transcritical small scale cycle operating with the CO_2 + SO_2 mixture.

Table 1
Cycle characteristics and non-idealities at design [32].

Parameter	Value at Design
Working fluid CO_2 + SO_2 composition [%molar]	82% CO_2
Pump Inlet Temperature [°C]	51
Subcooling Pressure Head [bar]	3
Pump Isentropic Efficiency	71%
Turbine Isentropic Efficiency	82.6%
Electromechanical Efficiency	99%
Turbine Inlet Temperature [°C]	550
Turbine Inlet Pressure [bar]	200
Turbine admission valve ΔP [bar]	1.5
ΔP Losses: PHE, REC_{HP}, REC_{LP}, Cond [bar]	3 / 2.37 / 0.87 / 2
Recuperator Minimum Internal ΔT [°C]	5
HTF: Inlet / Outlet Temperature [°C]	580 / 523
Ambient Temperature [°C]	40

Table 2
Cycle main variables and power balance at design [32].

Parameter	Value at design
Working fluid Mass flow rate [kg/s]	26.8
Pump Inlet Pressure [bar]	82.7
Pump mechanical Power [MW]	0.61
Recuperator Thermal Duty [MW_{th}]	11.9
PHE Thermal Duty [MW_{th}]	6.2
Turbine mechanical Power [MW]	2.45
Condenser Thermal Duty [MW_{th}]	4.28
UA Recuperator [MW/K]	0.20
Gross Cycle Efficiency [%]	30.4
Fan auxiliary consumption [kW_{el}]	46
Net system efficiency [%]	30.1

without oversizing it excessively. The mixture composition is defined in a preliminary analysis by maximizing the cycle efficiency at design conditions considering minimum and maximum temperature of 51 °C and 550 °C, respectively, and a maximum pressure of 200 bar. The properties of the mixture are computed with the equation of state embedded in Refprop v.10, previously validated against experimental data of the same mixture [24]. The reported net electric efficiency of this cycle is 30.1%: to better justify the adoption of this working fluid under these boundary conditions, the work also reports the performance of a solution based on sCO_2.

An analogous sCO_2 cycle has been simulated assuming the same hot source, adopting the same plant layout, with the characteristics and non-idealities reported in Table 1, including the very high cycle minimum temperature (51 °C): for this, a resulting 28.1% net system efficiency is estimated According to the numerical simulation, the corresponding sCO_2 cycle would have a compressor inlet pressure of 100 bar, optimized to maximize the cycle efficiency, without any subcooling (as expected for a cycle with supercritical compressor). Therefore, considering the net efficiency difference between the sCO_2 solution and the cycle of this work, the corresponding solution with sCO_2 would bring to a reduction in electric power produced of almost 7%, with a more rigid operation given the use of the compressor, especially at low ambient temperatures.

The T-s diagram and P-T diagrams of the investigated cycle at design conditions are shown in Fig. 2. It can be noted that the heat rejection (from 6 to 1) occurs in a very narrow working fluid temperature range (of around 26 °C, from T_6 = 77 °C to T_1 = 51 °C), due to the large enthalpy variation during the mixture condensation.

Being the knowledge of system internal volume of paramount importance to estimate plant off-design behavior, Table 3 reports the estimation of the lengths and internal volumes of each component and piping as provided by project partners. Regarding the material selection, piping is proposed to be in Inconel 617 on the high temperature side and stainless steel 316 L on the low temperature side: stainless steel is also considered for the condenser and the recuperator, while Inconel in the PHE. Considering the fluid properties and the components and piping volume, the small scale plant investigated in this work requires a total inventory of around 1379 kg of CO_2 + SO_2 mixture (82%molar in CO_2).

The design and characterization of the two turbomachinery for this investigated cycle is carried out by the turbomachinery manufacturer "Baker Hughes" [34], as partner of the EU H2020 DESOLINATION project: the pump is studied as a multistage axial machinery with variable speed (from approximately 2300 rpm to 4400 rpm, with a design condition of 3580 rpm), able to provide the necessary prevalence in a wide range of volumetric flow rate with a good efficiency, while the turbine is a multistage axial machinery operated with a fixed rotational speed of 17,000 rpm, reduced with a gearbox down to 1800 rpm to be coupled to a 4-poles generator. The turbine can be actively controlled through a throttling valve at its inlet, necessary to operate the cycle off-

Table 3
Details on the projected plant internal volumes and footprint. HP refers to high pressure, LP to low pressure.

Parameter	Value at design
Condenser: Pass length [m] / Volume [m^3]	16.2 / 2.32
REC HP: Channel length [m] / Volume [m^3]	1.5 / 0.13
REC LP: Channel length [m] / Volume [m^3]	1.5 / 0.13
PHE: Channel length [m] / Volume [m^3]	0.29 / 0.044
Piping: Conden. - Pump [m] / Volume [m^3]	11.0 / 0.190
Piping: Pump - HP Rec. [m] / Volume [m^3]	7.0 / 0.121
Piping: HP Rec. - PHE [m] / Volume [m^3]	2.3 / 0.019
Piping: PHE - Turbine [m] / Volume [m^3]	9.3 / 0.076
Piping: Turbine - LP Rec. [m] / Volume [m^3]	10 / 0.082
Piping: LP Rec. - Conden. [m] / Volume [m^3]	6 / 0.122

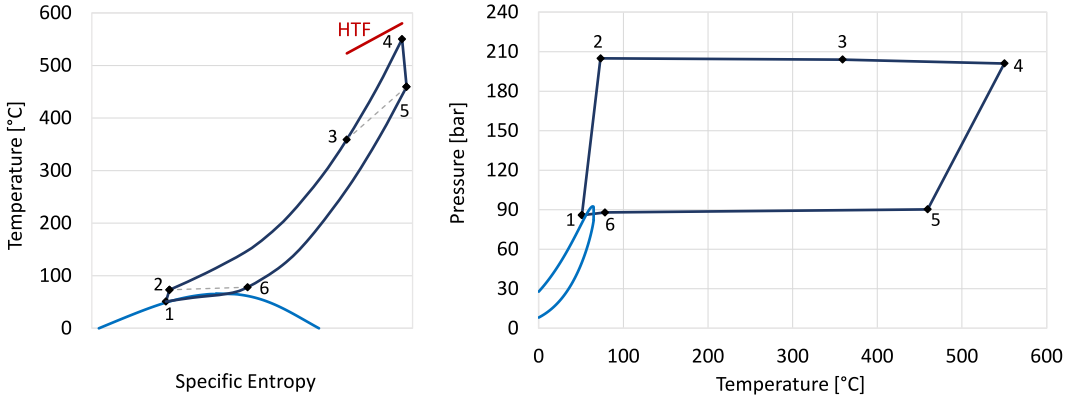

Fig. 2. T-s diagram (left) and P-T diagram (right) of the prospective small scale cycle investigated at design conditions: working fluid (dark blue), two phases saturation curve (light blue) and HTF (red). (For interpretation of the references to colour in this figure legend, the reader is referred to the web version of this article.)

grid. In addition, a trip valve and a bypass valve at turbine inlet and a non-return valve (check valve) at its outlet are foreseen, so that it can be possible to isolate the machinery both during emergency conditions and transients. Both the pump and the turbine are modelled in this work through off-design maps, reported in the appendix, provided by defining the pressure ratio and the total-to-static efficiency (that is assumed for the cycle simulations as the isentropic efficiency) as function of the reduced mass flow.

A preliminary sketch of the DESOLINATION plant layout, including the desalination section, is shown in Fig. 3.

The air-cooled condenser is modelled as multiple banks of tubes with 7 passes, where the air flows in crossflow with respect to the working fluid, considering the geometrical data and the 1-D model from previous works of the project [32,35]: the condenser is designed with axial fans at the maximum rotational speed in nominal conditions, allowing to reduce the air flow rate down to 20% of the nominal value during part load operation with variable speed motors. Electronically commuted fans of the condenser bays can allow for stepless velocity variation in that range: nevertheless, conditions below 20% of the fan speed are not considered as the fans also rely on the air movement as a cooling technique of the motor, and drastically reducing the cooling effect can be problematic at high ambient temperatures. Moreover, the geometrical features of the recuperator and PHE can be considered an innovative aspect being both manufactured as gyroidal-shaped printed circuit HXs (PCHE). In gyroidal-shaped channel, turbulence is enhanced and the heat exchange area is reduced with a consequent increase of the risks of salt solidification. To solve this issue the PHE is provided with electric resistances able to supply more thermal power to the solid structure in case of risk of solidification monitored with measurements of pressure drops and salt outlet temperature. Their geometrical characteristics and peculiar methodology for their 1-D thermal modeling was described in a previous work [32]. Details on the modeling of these crucial components are necessary, since their characterization and simulation in off-design conditions can substantially affect the behavior of the overall power cycle. All details about HX modeling are taken from the previous literature works of the DESOLINATION project and are also summarized and recalled in the appendix.

As the characteristics of the HTF pump and the two tanks of HTF are not defined yet, it is assumed that the HTF is able to be circulated from the design mass flow down to 50% of the nominal value, without facing any solidification issues due to its very high temperature (supposedly always around 523 °C, at the PHE outlet).

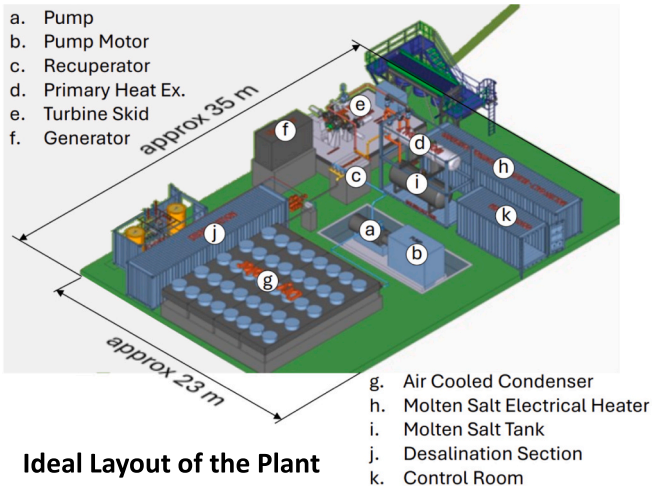

Fig. 3. Preliminary 3D representation of the prospective plant layout for the DESOLINATION demo plant. (Courtesy of Protarget AG).

3. Methodology for the off-design analysis of the transcritical power cycle

This section proposes the methodology adopted to carry out off-design simulations of the power cycle, including details on the numerical routine developed to simulate a constant inventory system.

Literature works on the off-design of sCO_2 cycles highlight that a variable inventory system, with inventory tanks connected to the cycle piping, is the solution that can ensure the highest efficiency at part load and different ambient temperature [36]: in this scenario the minimum pressure of the cycle can be optimized, but a slow response is expected [37]. An alternative to improve the responsiveness of the system can be found using a bypass of the turbine as inventory control method that momentarily keeps the inventory constant [38], a solution very fast to capture drastic variations of the load, but unable to lead to good cycle efficiencies. On the other hand, a fixed inventory sCO_2 cycle suffers conditions with ambient temperatures higher than the design value, pressurizing the loop and operating far from the best efficiency point of the turbomachinery. On this regards, the adoption of the mixture can help in defining a design point, at fixed inventory, with a high ambient temperature: as the critical temperature of the mixture is by definition higher than the cycle minimum temperature in a transcritical configuration, properly tuning the mixture composition of the transcritical cycle, design values of ambient temperatures can be set even above 40 °C with no strong penalization of cycle efficiency. Nevertheless, the efficiency improvement attainable using a mixture compared to the pure CO_2 remain strongly site-dependent and only an annual analysis with real weather data can assess the real performance gain of the innovative configuration.

Regarding the analysis on the $CO_2 + SO_2$ mixture of this work, in addition to the constraint of constant inventory, some other potentially limiting factors in off-design operation are included in the analysis:

1. The fluid at the pump inlet must be in liquid state, with a minimum level of subcooling equal to 3 bar, preventing cavitation and damage to pump blades. The subcooling section is not achieved in a dedicated component, but it occurs within the tubes of the main condenser itself, as already proposed in literature [32].
2. The fluid at the inlet of the condenser (i.e. the outlet of the recuperator at low-pressure side) should preferably be in vapor phase, as it is at design condition (referring to Fig. 2), avoiding two-phases flow in the condenser manifold, headers and piping that may cause liquid accumulation and phase separation (a problematic specific to blends). This could affect the composition of the circulating working fluid, uneven flow distribution in the heat exchanger and in unexpected behavior of the plant. A possible approach to deal with two-phase flow maldistribution in case of mixtures is to increase velocity and turbulence in the condenser distribution manifold: this however inevitably leads to larger pressure drops that may excessively penalize the system performance and, for this reason, not considered as an option in this work.
3. The maximum cycle pressure, at pump outlet, should be above the pressure of the mixture cricondenbar (around 100–110 bar), avoiding two-phases conditions in the recuperator at high pressure.
4. The maximum and minimum temperature of the HTF must be constant in any condition, keeping constant the temperatures in the cold tank and hot tank of the thermal energy storage (TES) as it is realistic for a CSP plant.

A flowchart of the system boundary conditions and control approach is shown in Fig. 4: the analysis of the cycle behavior in off-design is presented for ambient temperatures in the range from 10 °C to 40 °C, reasonable for the location of the demo plant, and thermal input from 100% of the design value to 50%, regulating the HTF mass flow rate [39].

The mass flow rate of coolant air (i.e. the air volumetric flow rate of

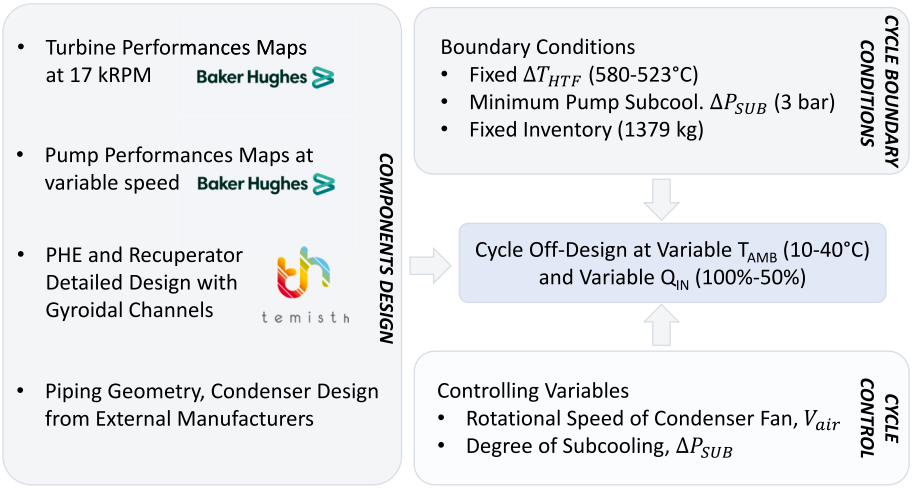

Fig. 4. Summary of the system input, boundary conditions and controlling variables.

the condenser fan) is the main control variable for every cycle condition, and it is varied to match the abovementioned boundary conditions, particularly the minimum subcooling degree. As mentioned, support in the modeling of the turbomachinery behavior has been received by Baker Hughes, whereas the HX manufacturer "Temisth" [39], as partner of the DESOLINATION project, has been involved in the design and development of the HX: details on the turbomachinery and HX characteristics and off-design simulations are available in the appendix.

The methodology for the analysis of the off-design conditions of the system is defined considering all the cycle boundary conditions and controlling variables: the model is developed in Python and it describes the system in steady state conditions. During each step of the iterative numerical procedure the heat exchangers are discretized to locally compute the convective heat transfer coefficient and frictional pressure drop with the appropriate correlations across each finite volume, depending on the flow rate, temperature and pressure of the fluid, according to the model reported in literature. Estimation of the inventory for each section of each HX is eventually obtained through the calculation of the mixture density.

Validation of the numerical models for each subcomponents is already available in literature, except for the detailed off-design characterization of the turbomachinery that is in this work implemented through operation maps (reported in Appendix) provided by the manufacturer (Baker Hughes), calculated with the support of computational fluid dynamics (CFD) analysis.

The PHE and recuperator gyroidal-shaped channels are modelled with a 1-D approach using conventional heat transfer correlations including correction coefficients tuned on the geometrical characteristics of the channel to account for the specific geometry: the agreement between the results of the 1-D model against the CFD results provided by the HX manufacturer (Temisth) is available in literature and discussed in the Appendix both on design conditions and off-design ones [32]. The results of the validation show that average errors on average convective heat transfer coefficients are below 5% in the whole set of off design conditions simulated with CFD simulations, varying both mass flow rates and pressure of the mixture in the channels.

The condenser design procedure is validated in a previous literature work [40], also discussed in the Appendix, comparing the condenser dimensions of the model (tube length, tube number and overall heat exchange area) with the results of design tools for air-cooled HX from industrial partner of the EU H2020 project SCARABEUS, showing very limited deviations. The same work also showed an experimental validation of the convective heat transfer coefficients of condensing CO_2-rich mixtures in the condenser tubes at similar range of pressures and temperatures of this study: the model adopted, already widely used in literature [41], predicts the experimental convective heat transfer coefficient with an average absolute error of around 5%.

The flowchart of Fig. 5 describes the simulation numerical structure: the core of the cycle solver is a system of eight non-linear equations to compute the specific off-design case with an imposed degree of subcooling (ΔP_{SUB}) and condenser fan speed (V_{air}), but without considering

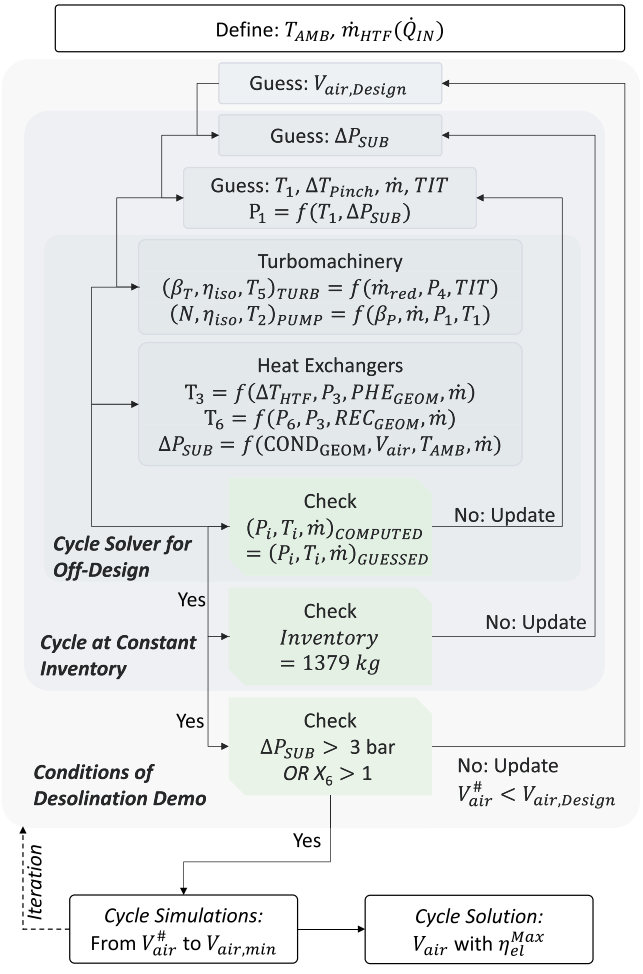

Fig. 5. Flowchart of the methodology to numerically compute off-design cycle conditions.

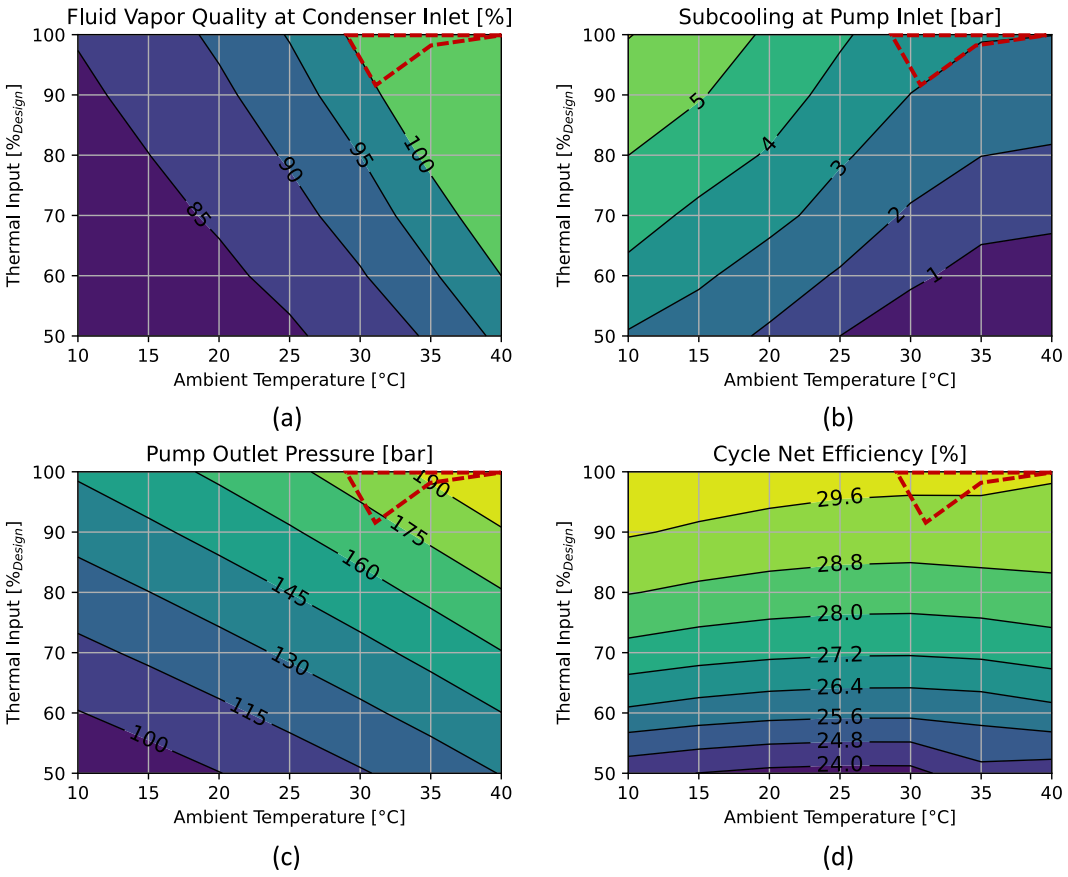

Fig. 6. Cycle behavior for the plant in off-design at rated condenser fan speed (V_{air_Design}): Vapor quality at condenser inlet (a). Subcooling degree at pump inlet (b). Pump outlet pressure (c). Cycle net efficiency (d). The red-dotted region identifies feasible operating conditions of the cycle ($X_6 = 100\%$ and $\Delta P_{SUB} > 3\ bar$). (For interpretation of the references to colour in this figure legend, the reader is referred to the web version of this article.)

constant inventory across the loop. The solution is reached varying the cycle minimum temperature T_1, cycle maximum temperature T_4, recuperator pinch point, mass flow rate and pressure drop in each heat exchanger. In this process the residuals to reach convergency on are: the difference between heat exchangers calculated area and design one, meaning channel or tube size and length (3 equations), the difference between calculated and assumed heat exchangers pressure drops on CO_2 side (4 equations) and the verification of operative point of turbine with respect to the off-design map (1 equations). At the outer solver level, the degree of subcooling ΔP_{SUB} is varied to match the inventory design value (1379 kg).

Once the cycle simulations at constant inventory are solved, the air flow rate (air velocity, V_{air}) is reduced iteratively until the minimum ΔP_{SUB} at pump inlet is targeted and single phase vapor flow is evaluated at condenser inlet, identifying a value denoted $V_{air}^{\#}$. Within the fan speed range between $V_{air}^{\#}$ and the minimum allowable air velocity $V_{air,min}$ (i.e. 20% of the nominal value), it is proposed a solution with a fan speed value leading to the cycle conditions with the maximum net efficiency (evaluated including the auxiliary consumption of the condenser fan). The air flow rate is hence considered as the last, extremely versatile, controlling variable.

4. Results: off-design of the DESOLINATION plant at constant inventory

The power plant behavior has been investigated in the whole operative envelope following the methodology described in the previous section, and the resulting thermodynamic conditions (temperatures, pressures) and working fluid mass flow rate in off-design conditions are shown in a series of maps proposed at variable ambient temperature ($T_{Ambient}$) and variable thermal input ($\dot{Q}_{IN}$). The first set of results has been obtained with a fixed condenser fan speed equal to the nominal one, whereas in the next section this assumption is relaxed to provide results able to respect the operative constraints related to minimum subcooling degree and no liquid fraction at condenser inlet, while at the same time optimizing the cycle net efficiency, as shown in Fig. 5.

The resulting trend of the net cycle efficiency of the plant at rated fan speed is proposed in Fig. 6, including the effect of the air condenser auxiliary consumption, along with the three main parameters to control in order to avoid problems in the cycle operation: the vapor quality at condenser inlet (X_6), the subcooling degree at pump inlet (ΔP_{SUB}) and the pump outlet pressure (P_2). These boundary conditions are not satisfied in the whole operating region except for a small region at ambient temperatures between 30 °C and 40 °C (identified with the red-dotted delimitation) and high heat input.

At low ambient temperatures the plant tends to operate with two phases flow at condenser inlet: considering the given sizing of the condenser and the constant thermal input, the mixture on the condenser is brought to lower pressures, making the flow at condenser inlet to falls in the two-phase region. At low thermal input the plant naturally moves to lower cycle maximum pressures (both at high pressure and low pressure side), due to the turbine behavior at low mass flow rate, needs

to accommodate a lower amount of fluid in the high density region to match the overall inventory condition, leading to a decrease in subcooling degree and pump cavitation risks. The net cycle efficiency is only slightly dependent on ambient temperature, while it is mostly affected by thermal input, ranging from around 30% at full load to around 24% at 50% load. The efficiency trend is also coherent with the trend of the pressure ratio across the turbine, as the large variations in pressure and flow rates at limited load deviates the turbomachinery behavior away from the design conditions. Finally, the cycle minimum pressure (at pump inlet) moves from the rated condition of 84 bar down to 40 bar at minimum thermal input and ambient temperature: its decreasing trend is coherent with the one of the maximum pressure (from 200 bar to about 90 bar), since the cooling capacity of the condenser fan, always at its maximum (being always at V_{air_Desgin}), reduces the minimum temperature levels and accordingly the pressure levels.

While typical pure fluid Rankine cycles show a large influence of cycle efficiency on the ambient temperature, they normally have large hotwell to accommodate the inventory in the two phase at any pressure and temperature. Since this is not a degree of freedom in the power cycle investigated, a decrease in ambient temperature drives an increment in the fraction of the inventory in subcooled conditions, a condition necessary to ensure the overall target inventory, through an iteration on the ΔP_{SUB} as presented in Fig. 5. Penalized by a higher subcooling degree at pump inlet, the solutions at low ambient temperature cannot benefit from a net gain in cycle efficiency with respect to the solutions at higher ambient temperature and same load.

The simulations at full fan speed inevitably lead to a decrease in minimum temperature as the ambient temperature decreases, bringing the cycle at conditions with two phase flow at condenser inlet for the large majority of the operating conditions. For a limited conditions in ambient temperature and load, at $T_{Ambient}$ below 20 °C and $\dot{Q}_{IN}$ below 60% of the design value, also the pump outlet pressure falls below the pressure of the cricondenbar (100 bar), introducing two phase flows at the cold side of the recuperator.

In conclusion, the operation of the system at constant inventory and rated condenser fan speed lead to not feasible operating conditions in almost the whole envelope, as it results in at least one unmet operative constraint (quality at condenser inlet or pump intake subcooling degree).

Before introducing the cycle results at optimized fan speed, the results at $V_{air}^{\#}$ are also shown (referring to the methodology of Fig. 5): proposed in Fig. 7, these trends highlights the cycle behavior in off-design with all boundary conditions met at the highest possible value of fan speed. Differently from the previous set of results, in Fig. 7 the X_6 is not shown since $V_{air}^{\#}$ is defined as the highest value of fan speed for which the flow at condenser inlet can be found at dew point, at saturated vapor conditions. The sole undesirable solution is found at minimum ambient temperature and load ($T_{Ambient}$ at 10 °C and $\dot{Q}_{IN}$ at 50%), where the minimum value of V_{air} is met (20% of the design value), while in all the other conditions the cycle can be operated with good flexibility meeting the operative constraints.

The fan speed drastically changes in this scenario, varying steeply both with load and ambient temperature, increasing the temperature difference between air and the working fluid at the most extreme off-design conditions as much as possible. The subcooling degree rises up to 9 bar at low ambient temperature: this is necessary to keep the inventory constant, allocating a higher fraction of working fluid in the liquid phase once the pressure levels of the cycle decrease in off-design and the average density of the fluid decreases. The increment in cycle efficiency by moving from the rated speed of the condenser fan (Fig. 6)

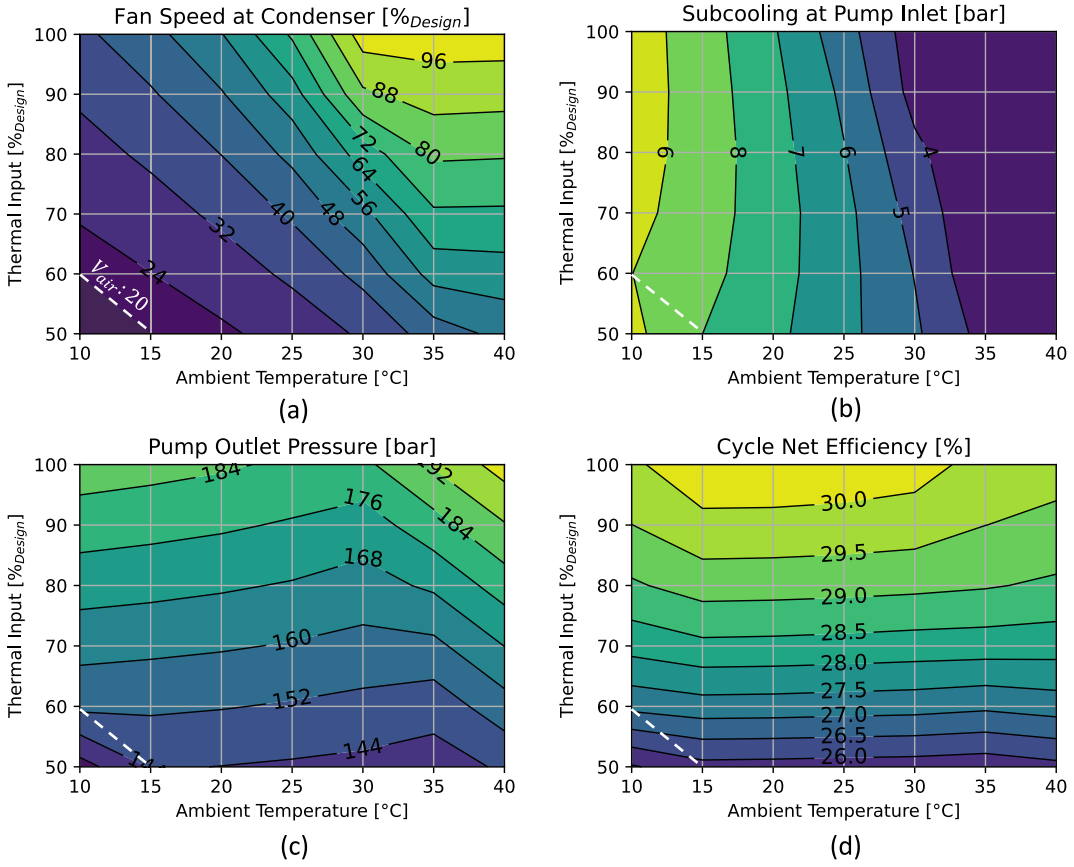

Fig. 7. Cycle behavior for the plant in off-design at maximum value of fan speed ensuring vapor phase at condenser inlet ($V_{air}^{\#}$): Trend of $V_{air}^{\#}$ (a). Subcooling degree at pump inlet (b). Pump outlet pressure (c). Cycle net efficiency (d). White dotted lines identify region with $V_{air}^{\#}$ at the minimum value (20% of V_{air_Design}).

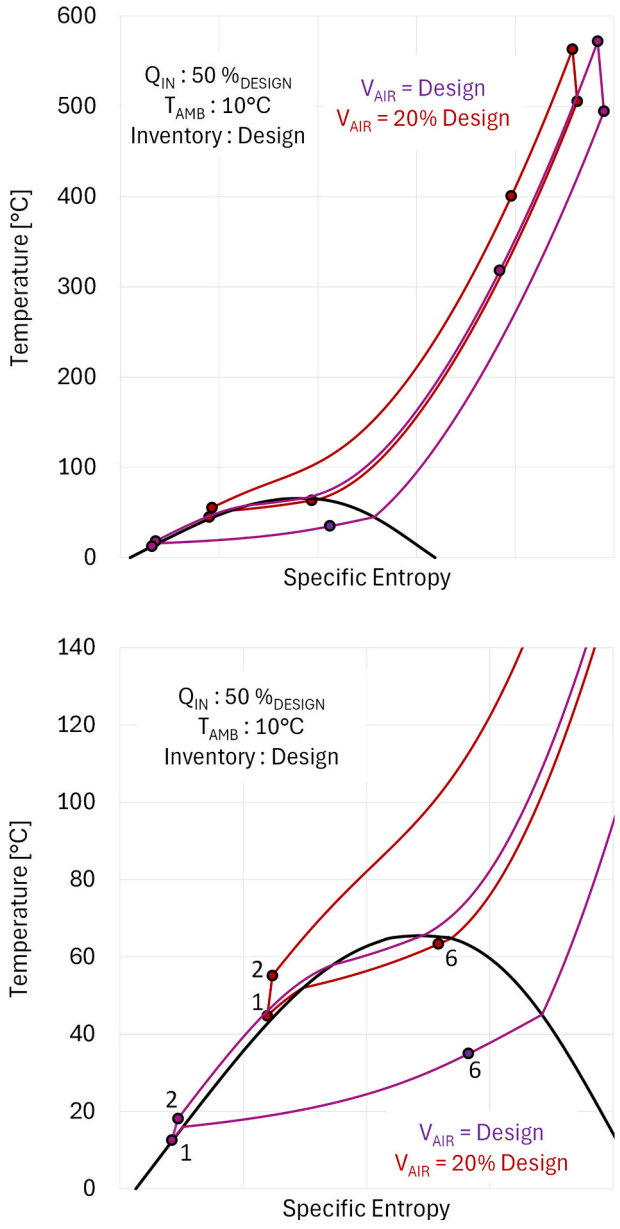

Fig. 8. Cycle Ts diagrams at minimum ambient temperature (10 °C) and thermal input (50%$_{Design}$) with different air flow rates: nominal V_{air_Design} (purple cycle), $V^{\#}_{air}$ corresponding to the minimum V_{air} (red cycle). (For interpretation of the references to colour in this figure legend, the reader is referred to the web version of this article.)

to $V^{\#}_{air}$ is noticeable, being from 0.5% at high load to 2% at the lower load. Finally, the maximum pressure is always found above 140 bar, far from the cricondenbar of the working fluid, as the lower flow rate of the cooling air also increases the temperature difference between the ambient and the cycle, with higher pressure levels on both sides of the cycle.

Extending the comparison between the cycle solutions at full speed of the condenser fans and the ones at $V^{\#}_{air}$, Fig. 8 depicts the T-s diagram of the most extreme case of the simulation domain (ambient temperature 10 °C and thermal input 50%) at both nominal (100%) air flow rate and at $V^{\#}_{air}$, corresponding to the minimum value of air flow rate (20%). Due to the low power rejected at the condenser, a pinch point of only about 2 °C is foreseen at the cold end of the air condenser at nominal fan speed, while this value grows to 35 °C at reduced $V^{\#}_{air}$.

It can be noted that the cycle with nominal air flow rate has a condenser inlet deeply in the two-phase region (vapor quality below 85%, already shown in Fig. 6), whereas the cycle simulated with a low condenser fan speed present higher cycle minimum and maximum pressures. The cycle pump outlet pressure at rated fan speed (88 bar) is also below the cricondenbar level of around 95 bar, at it was discussed in Fig. 6 and noticeable in the Ts diagram. Operating the cycle at higher pressure levels results in lower specific latent heat in condensation and pushes the condenser inlet close to saturated vapor conditions, increasing the working fluid mass flow rate and the temperature at PHE inlet.

4.1. Results: off-design simulations at optimized condenser fan speed

Previous results of off-design cycle simulations obtained at constant speed of the condenser fans entail problems with two-phase flow at condenser inlet (X_6 below 100%) and insufficient subcooling pressure difference (ΔP_{SUB}): tackling this issue, the previous section highlighted cycle simulations where both of these constraints were met by reducing the fan speed at $V^{\#}_{air}$.

Nevertheless, the optimal cycle conditions do not necessarily coincide with the fan speed value at $V^{\#}_{air}$, as pointed out in the methodology section. To demonstrate this, it is proposed a sensitivity analysis of the influence of the condenser fan speed on the main cycle variables of interest, shown in Fig. 9, at $T_{Ambient}$ of 25 °C and thermal input of 90%: it is evident that the $V^{\#}_{air}$ is 60%, bringing X_6 at 100% (dark curve in Fig. 9 (a)), while the optimal cycle efficiency can be found at V^{Opt}_{air}, at around 50% in this particular condition. A reduction in air flow rate, for a given $T_{Ambient}$ and $\dot{Q}_{IN}$, leads to two different effects: at first, the reduction of convective heat transfer coefficient on the air side, which is strongly affected by the air velocity, entails a higher average temperature difference between the air and the condensing mixture, whereas, on the other side, the lower mass flow rate of the coolant air implies a larger

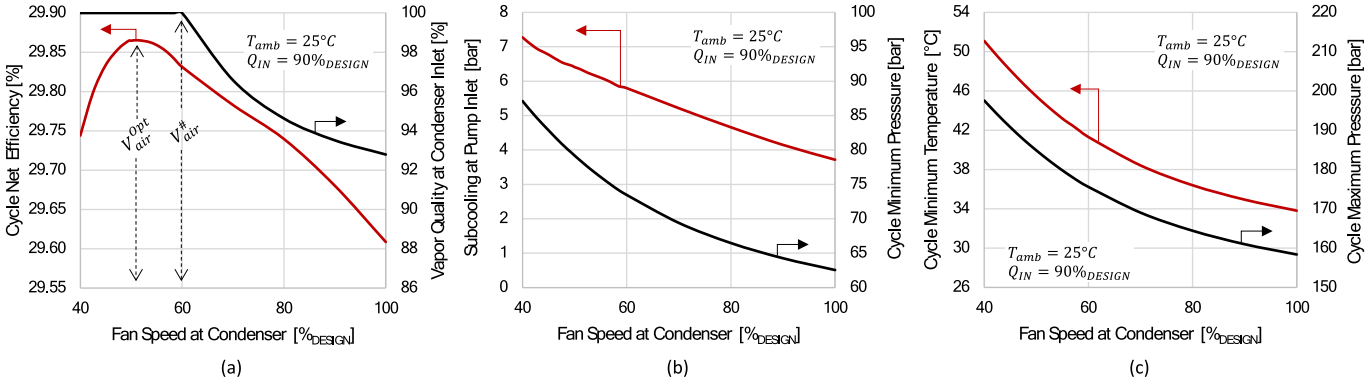

Fig. 9. Sensitivity analysis of the cycle behavior with a variation of cooling air flow rate: simulations for a single representative conditions of cycle off-design at $T_{Ambient}$ of 25 °C and thermal input of 90%.

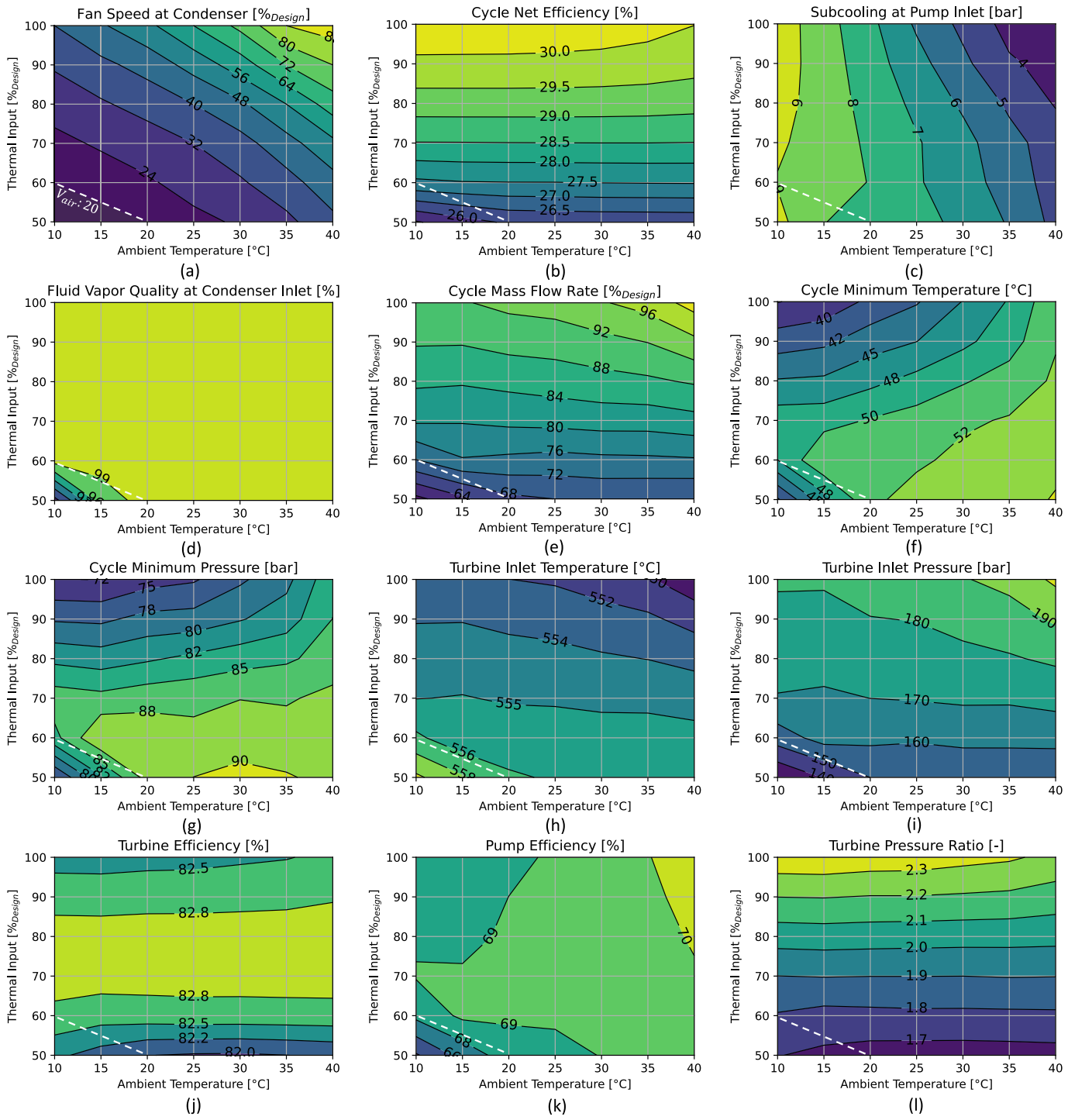

Fig. 10. Behavior of the cycle studied in this work in off-design at variable fan speed: results are presented for the value of V_{air} that maximizes the net cycle efficiency. White dotted lines identify region with $V_{air}^{\#}$ at the minimum value (20% of V_{air_Design}).

temperature variation of the air, reducing the relevance of the fan electrical consumption. Both effects push the cycle minimum pressure P_1 to higher values, with an increment in cycle minimum temperature T_1, matching the constant inventory constraint with a higher subcooling degree ΔP_{SUB}, as visible in Fig. 9(b) and (c).

The results presented in this chapter highlight the cycle operation with a condenser fan speed equivalent or below $V_{air}^{\#}$, being V_{air}^{Opt}, leading to the highest net cycle efficiency as explained in the methodology section in Fig. 5. Of this set of simulations all thermodynamic variables including temperatures, pressures and flow rates are shown in Fig. 10.

As visible in Fig. 10(a), representing the condenser fan speed that maximize the net efficiency, this decreases quickly from the design point with a reduction of both the thermal input and ambient temperature of the cycle, down to a region with $T_{Ambient}$ lower than 20 °C and $\dot{Q}_{IN}$ lower than 60% of design load (represented by a white dotted line), where it reaches the minimum value of 20% of the design value. Only in that specific region the mixture enters in the condenser in two phase flow, since at fixed V_{air} there is no degree of freedom available to match the boundary condition of dry flow at condenser inlet. It is noted that along all the simulation domain, the fan speed that maximizes the efficiency is

always below $V_{air}^{\#}$ of Fig. 7. The cycle efficiency, Fig. 10(b), has negligible dependency on ambient temperature, similarly to the mass flow rate of the cycle, and decreases from around 30.5% to 26% depending on the load, always above the one at full speed of the fan in Fig. 6. Comparing the cycle efficiency in Fig. 7 at $V_{air}^{\#}$ with the one at optimized fan speed in Fig. 10(b), only a very small deviation is noticeable. As mentioned in the previous section with results at $V_{air}^{\#}$, the cycle efficiency (Fig. 10(b)) always increase for increases of turbine pressure ratios (Fig. 10(l)). The turbine pressure ratio is slightly affected by ambient temperature and only increases from 2.28 at rated conditions up to 2.38 at full load and minimum ambient temperature. Differently, the impact of load is more relevant as the pressure ratio decreases down to 1.65 at the lowest thermal input (50% of the nominal) as a consequence of the sliding pressure off-design behavior of the turbine when operating at low mass flow rates.

The subcooling pressure head at pump inlet varies almost linearly from 3.5 bar to 9 bar with the ambient temperature, in analogy with the results proposed at reduced fan speed $V_{air}^{\#}$ of Fig. 7: this parameter is again used by the routine to match the overall inventory as proposed in Fig. 5.

The cycle minimum temperature T_1, Fig. 10(f), and pressure P_1, Fig. 10(g), conceptually linked by the subcooling degree at pump inlet ΔP_{SUB}, present similar trends by showing the highest values at low thermal input and high ambient temperature, with minimum values at high thermal input and low ambient temperature: the minimum pressure varies from around 90 to 73 bar, always below the cricondenbar of the mixture (i.e. around 94 bar), while the minimum temperature from 54 °C to 38 °C.

A minor sensitivity to the operating conditions is visible for the turbine inlet temperature *TIT* and turbine efficiency, in Fig. 10(h) and (j), whereas a strong variation of the maximum pressure P_4 is noted in Fig. 10(i), moving from around 200 bar at design conditions and decreasing almost linearly with $T_{Ambient}$ and $\dot{Q}_{IN}$, down to 140 bar where it drops to 125 bar in the region where V_{air} is constrained at 20% of the design value, still 30 bar above the cricondenbar. The efficiency of the turbomachinery present very little variations, with the pump efficiency always within 2 percentage points (between 68% and 70%, approximately), and the turbine one always between 82% and 83%.

It is necessary to highlight that at constant thermal input, constant inventory cycle experiences only minor variations in thermodynamic conditions when the ambient temperature decreases. This result is obtained thanks to a value of optimal V_{air} that decreases almost linearly with respect to $T_{Ambient}$ reductions. Differently from simulations proposed at V_{air_Design} in Fig. 6, this cases cannot thus benefit from a reduction in ambient temperature: even with a significant variation of ambient temperature from 40 °C to 10 °C, the cycle minimum temperature does not drastically change and decreases from 50 °C to 39 °C and 44 °C at maximum and minimum load respectively. Under these circumstances only a limited variation in cycle minimum pressure is obtained at a cost of a large increment of ΔP_{SUB}, leading to a larger share of inventory localized in the highest density region of the plant.

To deepen the analysis on the inventory distribution along the cycle components at variable ambient temperature, the results of Fig. 11 show the amount of inventory (in kg) in each region of the loop, according to the cycle simulations at full load, assumed as a representative load condition. While the highest share of the fluid inventory is always in the condenser and in the piping between condenser and pump, the phase distribution in the condenser tubes (volume and mass allocated in vapor, two-phase flow and subcooled liquid) changes remarkably at different ambient temperatures.

At high ambient temperature, a large fraction of the inventory in the condenser is in superheated vapor phase (around 250 kg, being 18% of the overall amount) similar to the amount of subcooled liquid in the condenser tubes found at liquid conditions while around 600 kg of inventory are in the two-phase condensing region.

As the ambient temperature decreases, the thermodynamic condition at condenser inlet approaches the saturated vapor region with an amount of inventory in superheated vapor phase that becomes negligible: from that condition, decreasing the ambient temperature further leads to an increase of the share of liquid. Regarding the high pressure side of the plant, the variation of mass of fluid in the PHE and recuperator at cold side is very limited since the operating maximum pressure moves only from around 200 to 182 bar in the two extreme conditions.

By comparing the inventory breakdown at full load for the two extreme ambient temperatures (10 °C and 40 °C), it is found that a similar amount of inventory in the subcooled liquid phase (around 250 kg) results in very different subcooling degrees, with a ΔP_{SUB} of around 9 bar at 10 °C and only 3.5 bar at 40 °C. This result can be motivated considering that in these conditions the optimal air flow rate ($\boldsymbol{V_{air}}$) changes remarkably being 90% and 40% the design value, at 40 °C and 10 °C $T_{Ambient}$, respectively. The condenser off design behavior induces a strong reduction of the cycle minimum temperature T_1 decreasing from 51 °C (at 40 °C ambient temperature) to 38 °C (at 10 °C), while the condenser pinch point at the condenser cold end increases from 11 °C to 28 °C, respectively. Due to the very different temperature difference between the air and the working fluid in the subcooled liquid section of the condenser, a higher share of the condenser tube volume is filled with liquid at high ambient temperature, inducing the trend of the inventory distribution in Fig. 11.

In conclusion, the results of this section highlight that the cycle

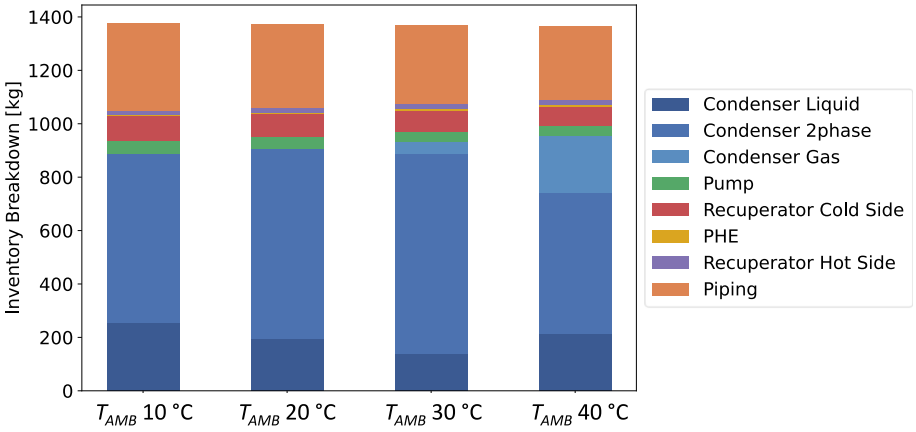

Fig. 11. Inventory distribution in off-design at full load and variable ambient temperature along the cycle components: simulations at optimized fan speed as shown in Fig. 10. Details on all the piping section volumes are reported in Table 3.

operation of a simplified plant architecture without variable inventory can be optimized in a wide range of operating conditions: this is done by achieving a sufficiently high efficiency while also respecting components operational constraints related to a minimum subcooling degree at pump inlet and a dry flow at the condenser inlet. This result is obtained by modifying the velocity of the condenser fan thus highlighting the need of having air cooled condenser units provided with electrical motors equipped with inverters and capable of a large range of velocity variation. The cycle operative parameters are expected to vary, especially in terms of pressure levels, but the need to keep a constant inventory level imposes a distribution where most of the working fluid remains in the condenser tubes.

5. Results: definition and calculation of the instantaneous settle out pressure (SOP) of the system

To conclude the analysis on the features and characteristics of the foreseen small scale plant, preliminary calculations of the instantaneous settle-out-pressure (SOP) are presented. The SOP is the pressure achieved by the working fluid inside the cycle once the mass flow rate stops and the two turbomachinery are halted: it is thus relevant to understand the behavior of the cycle during an emergency shut-down condition for example in case of turbomachinery trips. The instantaneous SOP of a closed loop plant inevitably falls in between the maximum and minimum cycle pressure before the event that caused the shutdown and it is crucial to understand if the established pressure may cause any damage to the components (valves, piping, heat exchangers) normally operating on the low pressure side of the system.

A rigorous analysis of the process must necessarily include a transient modeling of the whole system including the working fluid expansion (for the mass in the high pressure side of the plant) and the working fluid compression (for the mass in the low pressure side of the plant), including also the heat transfer of the fluid with the material of piping, valves and heat exchangers, the thermal dispersions and the thermal inertia of metal mass, insulation and molten salt on the hot circuit. The rigorous dynamic calculation is not in the scope of this work, also considering that the reliability of the approximate approach followed in this chapter has been already confirmed by literature works, for example applied to the pilot plant of the STEP project by comparing models and experimental data [42].

In this chapter the analysis from literature on the STEP project is resumed and extended, by calculating the SOP value for the small scale plant of this work, which differs remarkably from the STEP as it is an air cooled transcritical cycle where the large majority of the inventory is located in liquid phase in the condenser (at low pressure and low temperature) and in the piping section (as shown in Fig. 11).

Two main methodologies are proposed in this work for the SOP calculation, all of them assuming the initial conditions by splitting the whole loop into a set of finite elements (over one hundred), each one with an initial mass of the mixture, volume and initial thermodynamic properties, coherently to the thermodynamic conditions immediately before the plant shut-down as proposed in the previous chapters. In the final condition the pressure is the same for all the elements, while the other thermodynamic conditions are inevitably different since the shutdown process brings each element from the initial state to the final one: as a matter of fact, it is not possible to compute the final condition if not by either fixing a second thermodynamic property for each finite volume (other than pressure) or by imposing the type of process.

The first method (see left side of Fig. 12) assumes for each element that the mass and the entropy does not change (SOP_{isoS}) between initial and final condition, thus representing a case where the elements at high pressure increase in volume (expand) while those at low pressure reduce in volume (compress) in a reversible way. The final pressure is calculated iteratively by verifying that the overall system internal volume in final condition is equal to the initial one. The equations that describe the numerical problem are here reported from Eq. (1) to (4), where "i" denotes the i-th finite element of the discretization domain, valid both for the high pressure side and low pressure one. Each finite-element internal volume is reported as V_i, superscript HP and LP refers to the high-pressure and low-pressure side of the plant whereas the superscript "′" refers to the thermodynamic conditions after the shutdown of the cycle.

$$\forall i : s_i'^{HP}\left(T_i'^{HP}, SOP_{isoS}\right) = s_i^{HP}\left(T_i^{HP}, P_i^{HP}\right) \tag{1}$$

$$\forall i : s_i'^{LP}\left(T_i'^{LP}, SOP_{isoS}\right) = s_i^{LP}\left(T_i^{LP}, P_i^{LP}\right) \tag{2}$$

$$\forall i : m_i'^{HP} = m_i^{HP} \; and \; m_i'^{LP} = m_i^{LP} \tag{3}$$

$$\sum\left(V_i^{HP} + V_i^{LP}\right) = \sum\left(V_i'^{HP} + V_i'^{LP}\right) \tag{4}$$

The second method developed to compute the SOP (see right side of Fig. 12) represents a process where the heat transfer between the fluid and the materials is so enhanced that for each element the volume and the temperature of the working fluid is constant (SOP_{isoT}), before and

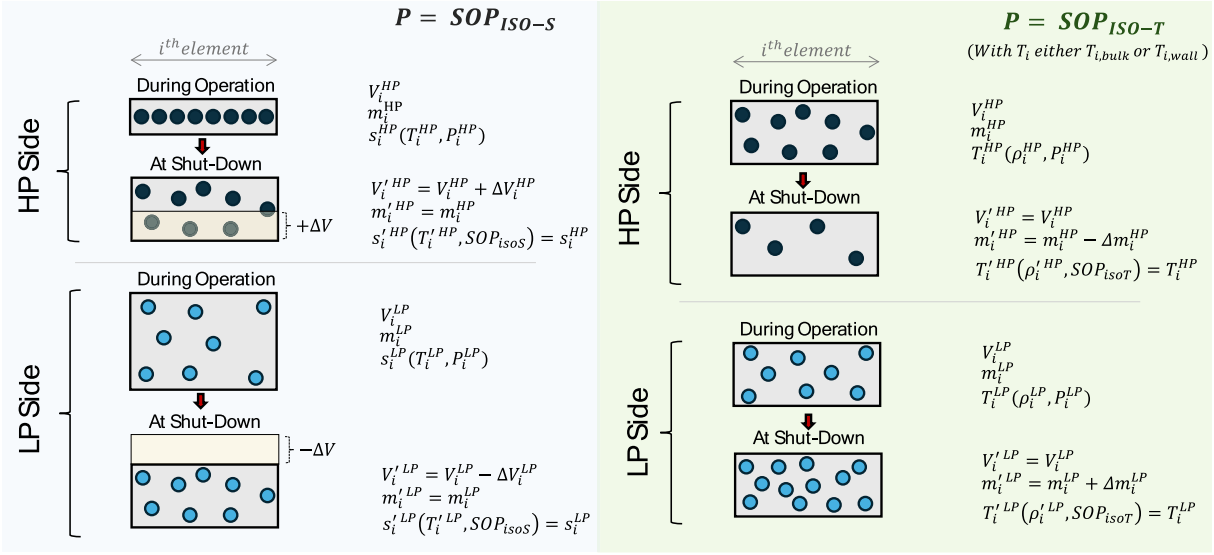

Fig. 12. Schematization of the methodologies for the SOP calculation under the assumption of: 1) constant entropy (left), and 2) constant working fluid temperature (right).

after the shutdown. This approach also involves that the thermal inertia of the metal (piping, valves, heat exchangers) is largely higher than the working fluid one. The final pressure is found iteratively to keep constant the overall fluid inventory (i.e. the overall negative variation of mass on the HP side is fully compensated by the mass gain in the LP side of the plant) and thus not considering venting or releasing a fraction of fluid to an external vessel. In this case it is not relevant to compute and compare any entropy variation, since the heat transfer between the fluid and the materials inevitably implies a change of entropy. The equations that describe the numerical problem of SOP calculations with isothermal approach are shown from Eq. (5) to Eq. (8).

$$\forall i : T_i'^{HP}\left(\rho_i'^{HP}, SOP_{isoT}\right) = T_i^{HP}\left(\rho_i^{HP}, P_i^{HP}\right) \tag{5}$$

$$\forall i : T_i'^{LP}\left(\rho_i'^{LP}, SOP_{isoT}\right) = T_i^{LP}\left(\rho_i^{LP}, P_i^{LP}\right) \tag{6}$$

$$\forall i : V_i'^{HP} = V_i^{HP} \; and \; V_i'^{LP} = V_i^{LP} \tag{7}$$

$$\sum\left(m_i^{HP} + m_i^{LP}\right) = \sum\left(m_i'^{HP} + m_i'^{LP}\right) \tag{8}$$

A graphical representation of the SOP is evidenced in the T-s diagram of Fig. 13, computed with the different methodologies obtained by considering a shut down from nominal conditions of the power cycle and nominal ambient temperature (40 °C): in this case the SOP_{isoT} is around 86 bar (green dotted line in the Ts diagram) and the SOP_{isoS} around 92 bar (blue dotted line).

Detailing these results from Fig. 13 at nominal conditions, considering the modeling with SOP_{isoS} it is interesting to note that total internal energy of the overall fluid inventory only changes by 1.04 kW, corresponding to a little equivalent thermal loss from the working fluid boundaries (considering, for example, that the thermal input is 6 MW at the PHE).

Additional calculations are thus carried out by considering slightly irreversible processes obtained by calculating the final entropy of each element as the initial one incremented by a little value $(1+\varepsilon)$. Results show that is sufficient a very little increase in entropy (ε=0.15%) to obtain a case with constant overall internal energy of all the inventory (SOP_{isoU}), even if the internal energy of each element still changes, representing an adiabatic case where the process of pressure equalization is faster than any heat transfer process with the material (piping, valves, heat exchangers) in contact with the working fluid. The SOP_{isoU} in this case is close to 93 bar, extremely similar to the SOP_{isoS}.

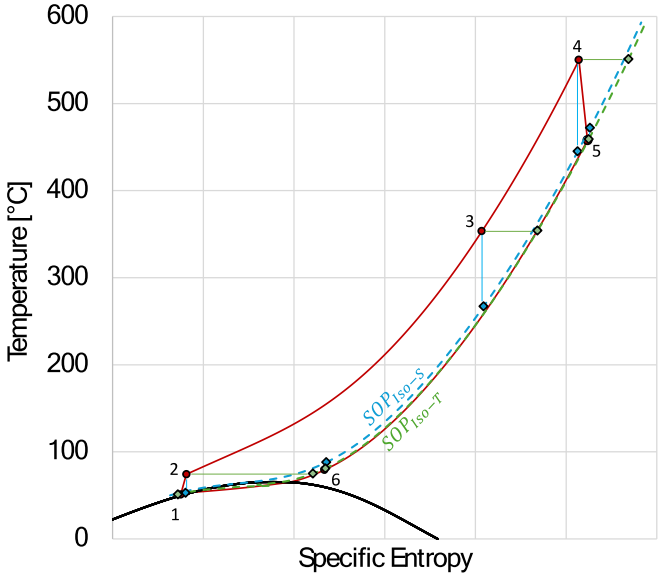

Fig. 13. Ts diagram of the cycle at nominal conditions and the respective SOP computed with the two different approaches.

All the approaches presented for the SOP calculation, including the SOP_{isoU}, have been numerically developed and tested across the whole range of ambient temperature (from 10 to 40 °C) and thermal input (from 50% to 100% the design value) proposed in Fig. 10. The resulting SOP values can be described by the three equations, from Eq. (9) to Eq. (11). As a general trend the SOP_{isoT} is very close to the minimum cycle pressure while the SOP_{isoS} and SOP_{isoU} are only slightly higher: nevertheless, all the calculated values are still pretty close to the minimum pressure, an effect caused by the significant fraction of fluid inventory at the lowest pressure and temperature inside the condenser and its relative piping sections. The SOP_{isoS} is always close to the SOP_{isoU}, indicating that the SOP_{isoS} calculations are developed with a methodology that is close to a condition of conservation of the overall internal energy of the fluid.

$$SOP_{isoT} \approx P_1 + 0.02\cdot(P_4 - P_1) \tag{9}$$

$$SOP_{isoS} \approx P_1 + 0.07\cdot(P_4 - P_1) \tag{10}$$

$$SOP_{isoU} \approx P_1 + 0.08\cdot(P_4 - P_1) \tag{11}$$

The multiplication factor 0.02 of the SOP_{isoT} is an average value of all the results between 0.011 and 0.023, while the factor 0.07 and the factor 0.08 are an average between the results of the various simulations ranging between 0.060 and 0.077 and between 0.069 and 0.088 for SOP_{isoS} and SOP_{isoU}, (respectively)

Finally, the evaluation of the SOP with the isothermal approach (SOP_{isoT}, crf. Right side of Fig. 12) is also revaluated by considering that the temperature at the bulk of each finite volume after shutdown (T_i') is kept equal to the wall temperature of the metal wall in each element before shutdown. Wall temperature (T_i^{wall}) is calculated considering the hot and cold fluid bulk temperatures and the heat transfer coefficients on both sides of the metal wall just before shutting down the plant. This approach strengthens the assumption that the thermal inertia of the metal mass has a preponderant contribution and bring the SOP_{isoT} very close to the cycle nominal minimum pressure (P_1) and in some cases even slightly lower than the design value. This can be motivated by the large share of inventory within the condenser that, under these hypotheses, cools down by around 3.5 °C, thus leading to an increment in density and a reduction in pressure.

The differences in the calculated SOP values are rather limited, and thus the operative SOP in the plant is expected to be close to the cycle minimum pressure. Considering that all the components, piping and welding at low pressure are rated at 130 bar no issues can be foreseen from safety and integrity perspective. This result is in agreement with the fact that the great majority of the inventory is at the cycle minimum pressure, in any off-design condition. The SOP_{isoS} or the SOP_{isoU} can be representative of the phenomena occurring inside the loop suddenly after the shutdown of the plant, with no time for the fluid to exchange heat with the tubes and piping material, whereas the SOP_{isoT} can characterize the system final condition after a slower shut-down allowing for a more effective interaction between the fluid and the material of the loop. However, a detailed transient analysis could be necessary for a more detailed evaluation of the process including all the effects related to real thermal inertia of materials and molten salt loop and for all those cases where the working fluid pump stays on as well and the air fans of the heat rejection heat exchangers.

6. Conclusions

A framework between academic and industrial partners has been developed within the EU H2020 DESOLINATION project, with the goal of provide insights on the characteristics and performances of a potential ambitious transcritical CO_2 mixture demo plant to be put in a relevant environment, specifically by simulating the boundary conditions of a CSP plant. The use of a novel working fluid, a condensing cycle configuration and the need to keep a constant inventory in the system

bring atypical challenges, particularly in off-design and part-load operation where specific constraints are required to ensure a safe and stable operation (i.e. limiting the liquid fraction at condenser inlet and imposing a minimum subcooling degree at pump inlet). As this work investigates SO_2 as dopant for CO_2, identified in previous literature works for its good cycle efficiency and proven thermal stability, the methodology followed in the analysis is replicable with any other dopant, preserving its broad applicability, along with the identification of the operative boundary conditions and approaches to overcome the limitations. Considering a warm location for a power cycle with air-cooling unit and solar salts as hot source, the power plant suggested with mixture is able to achieve 7% more electric power at design conditions with respect to the pure sCO_2 cycle at same boundary conditions, in addition to easing the off-design operation with a higher flexibility range, especially at low ambient temperature (down to 10 °C) and limited load (50% of the design value).

The outcomes of the work can be summarized as follows:

- The off-design analysis shows that a feasible operation in the whole envelope would not be possible without the possibility of precisely controlling the air-cooled condenser fans velocity over a wide range, whereas operating the condenser at constant air mass flow rate would lead to unfeasible conditions characterized by recuperator outlet in two-phase flow and unacceptably low subcooling degree.
- Reducing the fan speed also brings the solution to a condition of maximum net cycle efficiency, higher level of subcooling and higher vapor quality at condenser inlet. Only the simulations at extreme off design condition (50% load and 10 °C ambient temperature) depicts a problematic cycle condition due to a small fraction of residual liquid content at the condenser inlet, even at minimum fan speed. Possible alternative solutions to be investigated in next follow up activities can include the switching off of some fans, furtherly reducing the air flow and the effective heat transfer area.
- An important outcome is represented by the good cycle efficiency over the whole operating envelope also in cases where fan velocity is reduced with an increase of cycle minimum pressure. The cycle efficiency drops by around 3.5 percentage points from nominal to minimum load, from around 30% to around 26.5% that represents a limited penalization considering the achieved minimum load, highlighting the capability of this cycle architecture to provide a wide flexibility from power production perspective. Differently, the effects on cycle performance of a reduction in ambient temperature is rather limited, as the optimal constant inventory system converges to a solution where the cooling air fan speed is reduced drastically at low ambient temperature, keeping similar the thermodynamic of the cycle in compliance with a constant inventory operation.
- Plant stop conditions have been evaluated by calculation of the settle out pressure with two different methodologies in case of instantaneous emergency shutdown, proposed as approximate methodologies to compute the phenomena of the fluid alterative to a more accurate transient analysis. If the shutdown is rapid and no heat exchange is modelled between the component materials and the working fluid, the settle out pressure will be approximately 7% of the way between the operational low and high pressures. In the case when the working fluid exchange heat with the surrounding material, the settle out pressure is significantly closer to operational low-pressure value (2% between low pressure and high-pressure value). This results mainly depend on the distribution of internal volume inside the cycle various components.

Future works can provide more insights into the modeling of the plant shut-down with a transient analysis, expanding the results of this work. Additionally, an experimental campaign on closed loop is foreseen in the near future to measure the settle out pressure of CO_2-loop in a relevant environment. From a material compatibility point of view, additional studies on the sulfur dioxide interaction with the metals can further support the working fluid choice. Finally, future works could propose an interesting comparison by simulating the cycle conditions and operational domain of a variable inventory loop, at same boundary conditions, understanding if the possibility to extract and reinject working fluid leads to an enhanced and widened admissible operative region and focusing on the difference in the resulting cycle performances.

CRediT authorship contribution statement

Matyáš Junek: Formal analysis, Investigation, Methodology, Software, Visualization, Writing – review & editing. **Ettore Morosini:** Conceptualization, Data curation, Formal analysis, Investigation, Methodology, Software, Visualization, Writing – original draft, Writing – review & editing. **Marco Astolfi:** Conceptualization, Investigation, Methodology, Supervision, Writing – review & editing. **Giampaolo Manzolini:** Conceptualization, Funding acquisition, Project administration, Supervision, Writing – review & editing.

Declaration of competing interest

The authors declare that they have no known competing financial interests or personal relationships that could have appeared to influence the work reported in this paper.

Acknowledgements

This paper is part of the DESOLINATION project that has received funding from the European Union Horizon 2020 research and innovation program under grant agreement No. 101022686.

This paper is part of the ISOP project that has received funding from the European Union Horizon MSCA 2020 research and innovation program under the project No. 101073266.

This paper is part of the project HICLOPS “High-medium temperature closed power cycles for waste heat recovery and renewable sources” that has received funding from the MUR Progetti di Rilevante Interesse Nazionale (PRIN) Bando 2022 under grant No. 2022HMZ39A.

Appendix A. Appendix: details on the numerical models for simulation of the cycle components

This appendix describes the numerical routines and procedures to model the cycle components both at design and off-design conditions.

A.1. Modeling approach of recuperator and primary heat exchanger

The PHE and the recuperator of the cycle are developed by the Temisth [39] in the frame of DESOLINATION project. A gyroidal-shaped channel type heat exchanger has been developed, shown in Fig. A1, and adopted as periodic geometry for both the PHE (Primary Heat Exchanger) and the recuperator. This geometry was already investigated in literature as a possible solution [43] to enhance the heat transfer convective coefficient and the compactness of the heat exchanger with respect to conventional sCO_2 equipment based on PCHE (Printed Circuit Heat Exchangers) with straight

channel [44].

The periodic gyroidal structure of the recuperator is modelled and simulated in CFD by Temisth along the channel axial coordinate up to its total length of 1500 mm. Flow passage area (perpendicular to the axial direction) is equal to of 12.49 mm^2 for each of the two sides of the heat exchanger. Considering the overall cycle mass flow rate and the recuperator heat duty, 6945 parallel countercurrent channels are needed. Analogous considerations can be made for the PHE relying on same periodic gyroidal structure and elementary geometry: for this heat exchanger channels total length is 290 mm and 2328 channels are required in parallel.

An experimental validation of the heat transfer capability of the projected geometry has not been carried out yet at this stage and their numerical modeling is based on CFD simulations already presented and discussed in previous publications of the DESOLINATION consortium [32].

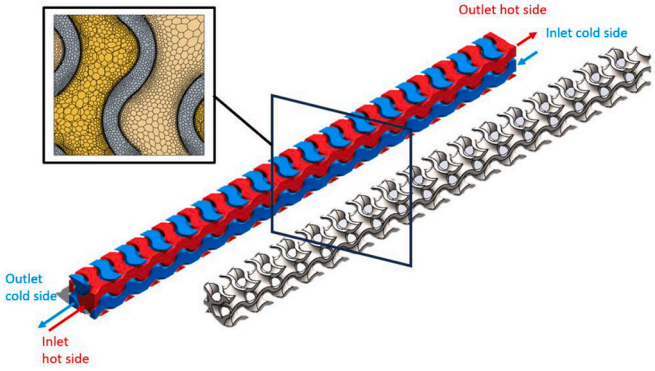

Fig. A1. Gyroidal shaped channel type used for PHE and recuperator of the cycle: mesh in CFD analyzed by Temisth [39] (top left), flow passage area with hot and cold fluid domain (yellow areas) and solid metallic matrix (grey areas). Figure adapted from literature [32]. (For interpretation of the references to colour in this figure legend, the reader is referred to the web version of this article.)

In the design phase, the model takes as input the thermodynamic characteristics at inlet and outlet of both hot and cold flows, along with the channel characteristics (except for its length). The simulations of these two HXs are developed in this work by considering a 1-D surrogate model of the HX developed in Python with the aim at reducing the computational efforts compared to CFD simulations and adopting the methodology already presented in previous study [32]. More specifically the surrogate 1-D model adopted starts from a consolidated model for straight channels PCHE where the semicircular channel dimensions have been set to match the following characteristics of the gyroidal shaped HX to be simulated: i) the cross-sectional area of each channel, as mentioned equal to 12.49 mm^2, ii) the velocity of the working fluid perpendicular to the cross-sectional area at design conditions, iii) the same wall thickness (0.6 mm) and material (Inconel 617), iv) the same heat transferred per channel, and finally, v) the same temperature and pressure at the inlet and outlet of the channel. By assuming the same input and output temperatures, the pinch point is also imposed, since it occurs at the cold-end of the channel for the design condition.

As output, the design model returns the length of each finite element, thus the overall length and the overall heat transfer area of the 1-D channel that aims to replicate the behavior of the gyroidal shaped one. The discretization adopts cold fluid fixed temperature variation in each element and thus a heat transferred in each element depending on the local value of fluid specific heat. Heat transfer coefficients are locally calculated with the procedure reported below while pressure drops are always imposed although corrected in off design conditions.

To ensure having a simulated heat exchanger with the same overall heat transfer area – and thus same internal volume and same metal mass - of the gyroidal heat exchanger designed by Temisth a correction factor on calculated local heat transfer coefficients is required since specific correlations for this channel geometry are not available. The approach proposed is to first calculate the local heat transfer coefficient as for a straight channel in PCHE heat exchangers ($HTC_{Convective}^{1D-Straight}$) adopting the Gnielinski correlation for the Nusselt number [45], reported in Eq. (A1) and then fitting a multiplicative correction factor $f_{Correction}^{HTC,CFD}$, in Eq. (A2) to calculate the equivalent heat transfer coefficient for the gyroidal geometry ($HTC_{Convective}^{Gyroidal}$) and match the total heat transfer area provided by the manufacturer. The procedure is repeated for both the PHE and the recuperator leading in both cases a correction factor ($f_{Correction}^{HTC,CFD}$) at design condition, "A" parameter in Eq. (A3), equal 4.5 for the mixture and 3.6 for the molten salt demonstrating the potential in heat transfer enhancement provided by such geometry.

The same procedure is repeated also for the results of other three CFD simulations allowing fitting the correction factor in different operating conditions. For the recuperator, a set of three off-design CFD simulations covering a wide range of pressures (from 205 to 165 bar on the cold side, from 90 to 75 bar on the hot side) and mass flow rate (from 100% of the design value to 60% of the design value), resulting in the formulation of the correction factor for the recuperator dependent on the mass flow rate and resulting independent from the fluid pressure. Analogous evaluations are made for the PHE, with additional CFD simulations provided by Temisth.

$$Nu = \frac{(f/8)\cdot(Re-1000)Pr}{1+12.7\cdot(f/8)^{1/2}\cdot(Pr^{2/3}-1)} = HTC_{Convective}^{1D-Straight}\cdot\frac{d_{hyd}}{k} \tag{A1}$$

$$HTC_{Convective}^{Gyroidal} = HTC_{Convective}^{1D-Straight}\cdot f_{Correction,Mixture}^{HTC,CFD} \tag{A2}$$

$$f_{Correction}^{HTC,CFD} = A + 0.1\cdot(100\% - \dot{m}_{WF}[\%]) \tag{A3}$$

The proposed 1-D surrogate model, including the proper correction coefficients $f_{Correction}^{HTC,CFD}$, is able to compute the average convective HTC on both sides of the HX within 5% of deviation for all the CFD results provided, including the design cases and the off-design ones.

Pressure drops are imposed in design condition and corrected in off-design adopting the correlation in Eq. (A4) where exponent 1.75 has been fitted on the various CFD results. In both design and off design pressure losses are distributed linearly in the heat exchanger flow paths, being a reasonable assumption considering that little relative pressure drops have a limited impact on local properties.

$$\Delta P_{OFF} = \Delta P_{DESIGN} \bullet \left(\frac{\overline{\rho}_{DESIGN}}{\overline{\rho}_{OFF}}\right) \bullet \left(\frac{\dot{m}_{OFF}}{\dot{m}_{DESIGN}}\right)^{1.75} \quad \text{(A4)}$$

Fig. A2 shows the methodology adopted for the thermal model for both the design and the off design of the gyroidal channel HXs from a numerical point of view. The routine iterates varying the outlet temperature from the channels to change the heat duty and match the heat exchanger total area at the design value. In some off-design conditions, the working fluid on the low-pressure side on the coldest section of the recuperator may condensate. Under these circumstances the Gnielinski correlation cannot be considered valid, therefore the Cavallini model for the calculation of the convective HTC of two-phase condensing mixtures is adopted [41]. This correlation was experimentally validated on a reference CO_2 mixture in a test rig in TUW [40].

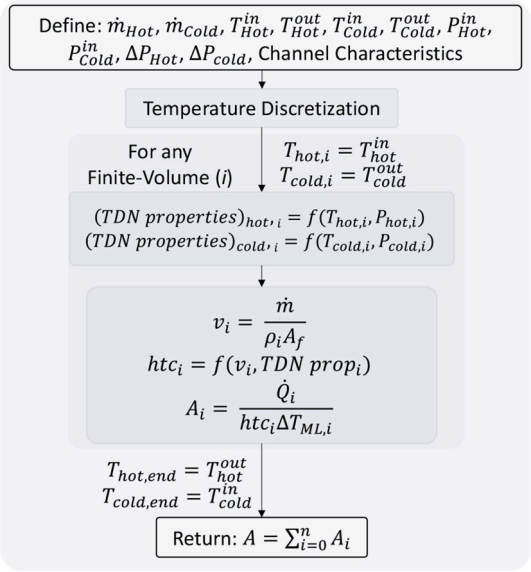

Fig. A2. Simplified flow diagram for the design and off-design of the gyroidal-shaped HX (PHE and recuperator).

A.2. Modeling approach for air-cooled condenser

An accurate modeling of the heat transfer rate inside the condenser tubes is crucial in understanding how the fluid is distributed across the loops and strongly affects off design calculations especially for constant inventory cycle. The sizing of the condenser in design conditions is carried out according to the model already proposed in a previous work on CO_2-mixtures, part of the SCARABEUS project [35] where a finned-tube condenser, with 7 loops per tube and air in crossflow with respect to the working fluid has been selected, as shown in Fig. A3.

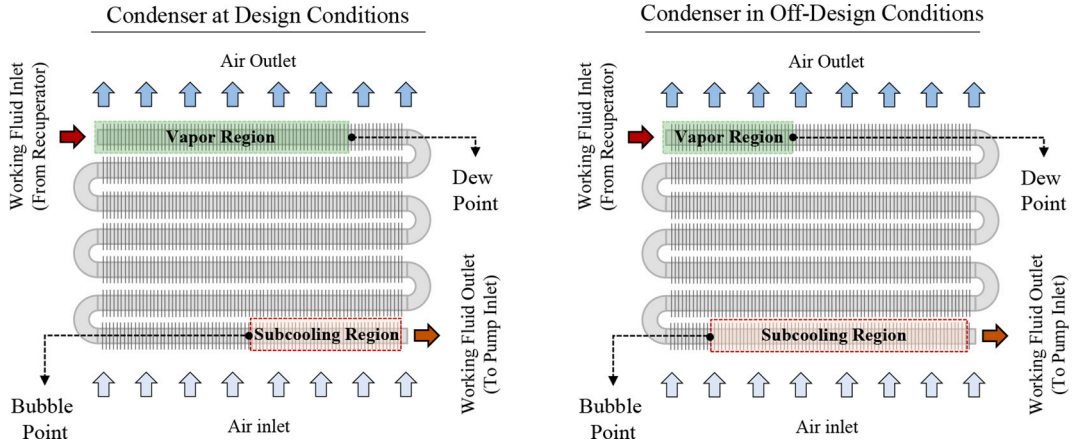

Fig. A3. Representation of the modelled crossflow air-cooled condenser. Qualitative behavior of the distribution of the mixture in the tube at design conditions (left) and off-design conditions (right).

Fig. A4 (a) describes the numerical routine for the sizing of the condenser tube geometry at rated condition.

Firstly, the design inputs such as inlet and outlet temperatures and pressures are provided to the model, along with the mass flow rate of the mixture and the air velocity. Also, the geometrical characteristics of the tubes, except for their length, are considered such as fins type and dimensions (area ratio equal to 27.3), tube diameters, materials.

The condenser computation routine reported in Fig. A4 (c) starts guessing the overall tube length and discretizes the tube in multiple finite volumes for each of the seven passes ("j" subscript) and each finite element along the axial coordinate ("i" subscript).

For any finite volume, the temperature variation of the working fluid in the tubes is guessed allowing to calculate the heat transferred ($\dot{Q}^{WF}_{i,j}$) from the working fluid to the air at given pressure and mass flow rate. The overall tube is divided into 140 finite volumes (20 per loop), modelled with

different approaches, according to the thermodynamic state of the mixture: superheated vapor, two-phase flow or subcooled liquid. In the vapor and liquid region, the Gnielinski correlation is adopted [45], whereas the Cavallini model for condensing mixture is used in the condensing region [41]. The frictional pressure drop is evaluated for each finite-element adopting the Chen friction factor in single phase conditions [35], and the Del Col model for the two-phase condensing flow [46], along with the Grimison correlation for the convection on the air side [47].

As the energy balance of the i,j-th element is defined on the working fluid side, the thermal model is run by computing the overall heat transfer coefficient ($U_{i,j}$). Once $U_{i,j}$ is computed, it is used to estimate the thermal power exchanged between the mixture and the air side with the $\epsilon - NTU$ method ($\dot{Q}_{i,j}^{NTU}$), comparing this value with the one previously computed ($\dot{Q}_{i,j}^{WF}$). Procedure starts from the heat exchanger cold end and moves from one element to the subsequent one once the heat duty of the actual i,j-th element is the same when computed with the two approaches.

Once a single condenser tube is simulated the temperature and pressure profile along the i,j coordinates both for the working fluid and the air are available. In design mode, the routine iteratively changes the tube length and the number of tubes checking if the overall temperature variation of the working fluid across the condenser and the relative pressure drop match the values defined at nominal conditions. In case this is not satisfied, the routine updates tubes length and number until convergency.

The condenser resulting from this procedure adopts 58 tubes with internal diameter of 21 mm and external diameter of 27 mm, each one 114 m long. The air is delivered to the condenser by axial fans powered by electrical motors with inverter: the air face velocity at design fan rotational speed is 3.19 m/s, incident perpendicularly to the tube, leading to a pressure drop on the air side of 100 Pa, computed considering the fin characteristics [35].

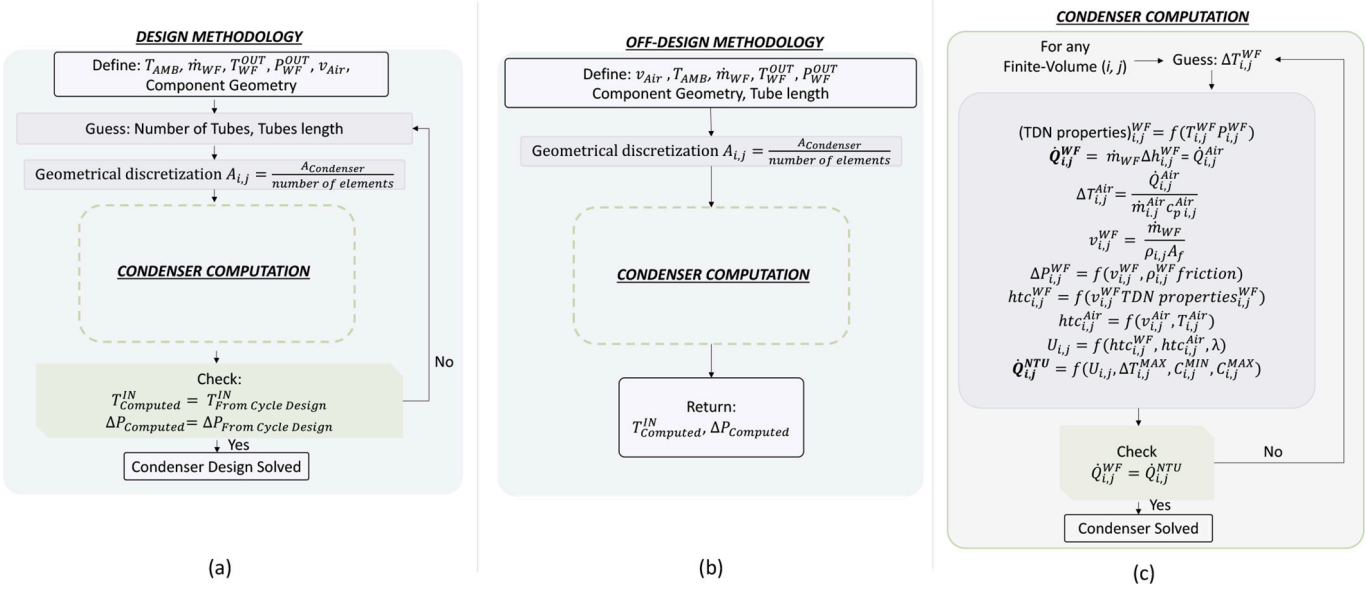

Fig. A4. Flow diagram for the design and off-design of the condenser.

Fig. A4 (b) describes the routine adopted for the condenser off-design. In this case the geometry of the tube, including its length and diameter are known as well the inlet and outlet conditions of the working fluid and the mass flow rate. The condenser calculation numerical routine is the same already described and reported in Fig. A4 (c) and calculates the working fluid inlet conditions (both temperature and pressure). The returned parameters are then used in the off-design solver to determine residuals for the fsolve algorithm described in section 3 and Fig. 5 of the manuscript.

For a complete overview of the equations used, the methodology and models adopted for the simulations of the crossflow air condenser, reaching convergency on certain operating conditions, please refer to the previous literature works on this topic [35,40].

A.3. Modeling approach and off design maps for the turbine and the pump

The operative maps of both the pump and the turbine are shown on non-dimensional axis normalized on nominal value of the corresponding quantity as provided by Baker Hughes in the design process of those components. Turbomachinery has been designed considering the working fluid of interest, the $CO_2 + SO_2$ mixture, at the design composition (82%mol CO_2) and modeling thermophysical properties in Refprop v.10, in compliance with the other calculations in this paper.

The pump is characterized by its pressure head curve, depicted in Fig. A5, as function of the volumetric flow rate at pump inlet and the rotational speed (N): the volumetric flow rate is evaluated considering the mass flow rate and the mixture density, in the range between 700 and 900 kg/m^3 for all the operative conditions considered in this study. The rotational speed of the pump is controlled in a range from +5% (maximum) to −36% (minimum) of the design value, to match instantaneously the required pump head at the desired volumetric flow rate. In addition, the trend of the pump efficiency is provided in the figure (dotted lines). At any given cycle operating condition (i.e. a combination of pressure head and volumetric flow rate), the pump required rotational speed and efficiency are thus univocally defined.

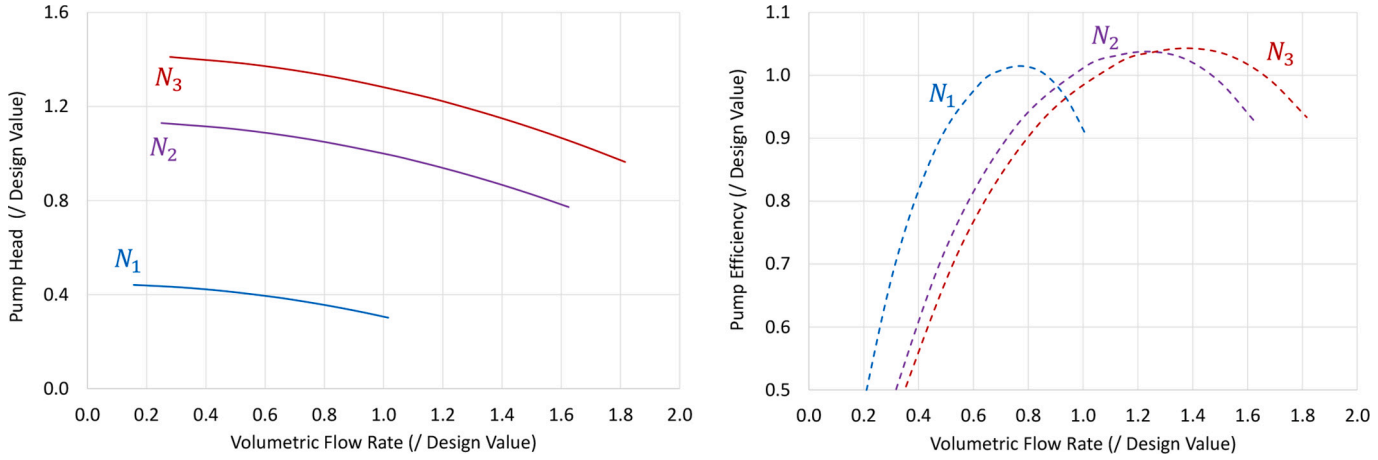

Fig. A5. Trend of the pump efficiency (left) and pump head (right) in off-design for the demo plant proposed in this study: results provided at constant rotational speed "N", in rpm. (© 2026 Baker Hughes Company - All rights reserved).

The axial turbine, differently from the pump, is operated at fixed rotational speed during operation (17,000 rpm), reduced with a gearbox to 1800 rpm to be coupled to a 4-poles generator. During the start-ups of the plant (i.e. cold start-up and warm start-up) its rotational speed is regulated from a minimum value to the design value of 17,000 rpm. The turbine performances are calculated at various reduced rotational speed N_r, defined as in Eq. (A5).

$$N_r = \frac{N}{\sqrt{TIT}} \tag{A5}$$

The turbine will be actively regulated through a trip and throttling valves at its inlet, necessary to operate the cycle off-grid and match the desired rotational speed. In addition, a turbine bypass valve and a non-return valve (check valve) at its outlet are present, so that it will be possible to isolate the machinery both during emergency conditions and transients. At any given reduced rotational speed N_r, the trend of the total-to-static efficiency is provided, shown in Fig. A6 (left), as function of the reduced mass flow rate at its inlet ($\dot{m}_r$) calculated as reported in Eq. (A6) considering only the main flowpath of the turbine stages in the analysis, avoiding the influence of valves, diffusers or additional localized pressure losses. Consequently, in this work it is assumed that the isentropic efficiency can be mimicked by the total-to-static efficiency, not considering the recovery of kinetic energy in the turbine diffuser.

$$\dot{m}_r = \frac{\dot{m} \cdot \sqrt{TIT}}{P_{IN}} \tag{A6}$$

Fig. A6 (right) depicts the expansion ratio of the fluid across the turbine for various reduced rotational speed N_r: this value refers again only to the flowpath of the machinery, and it does not include localized pressure losses at its inlet and outlet.

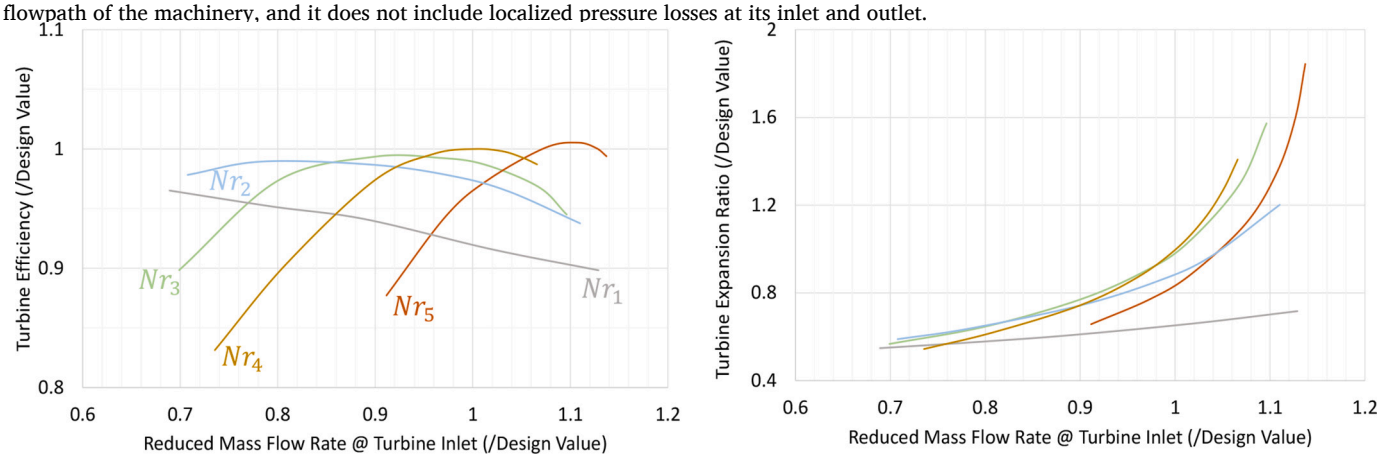

Fig. A6. Trend of axial turbine efficiency (left) and the expansion ratio (right) as function of the reduced mass flow rate at turbine inlet, in off-design, for the demo plant proposed in this study: results provided at constant reduced rotational speed "Nr", in rpm/$K^{0.5}$. (© 2026 Baker Hughes Company - All rights reserved).

Data availability

Data will be made available on request.

References

[1] M.T. White, G. Bianchi, L. Chai, S.A. Tassou, A.I. Sayma, Review of supercritical CO_2 technologies and systems for power generation, Appl. Therm. Eng. 185 (2021), https://doi.org/10.1016/J.APPLTHERMALENG.2020.116447.

[2] G. Baglietto, S. Maccarini, A. Traverso, P. Bruttini, Techno-economic comparison of supercritical CO_2, steam, and organic Rankine cycles for waste heat recovery applications, J. Eng. Gas Turbines Power 145 (4) (2023), https://doi.org/10.1115/1.4055727/1146452.

[3] F. Crespi, D. Sánchez, J.M. Rodríguez, G. Gavagnin, Fundamental Thermo-economic approach to selecting sCO_2 power cycles for CSP applications, Energy Procedia 129 (2017) 963–970, https://doi.org/10.1016/J.EGYPRO.2017.09.215.

[4] G. Angelino, Carbon dioxide condensation cycles for power production, ASME J. Eng. Power 90 (3) (1968) 287–296, https://doi.org/10.1115/1.3609190.

[5] V. Dostal, M.J. Driscoll, P. Hejzlar, A Supercritical Carbon Dioxide Cycle for Next Generation Nuclear Reactors, Technical Report MIT-ANP-TR-100, 2004, pp. 1–317, doi:MIT-ANP-TR-100.

[6] P. Wu, et al., A review of research and development of supercritical carbon dioxide Brayton cycle technology in nuclear engineering applications, Nucl. Eng. Des. 368 (2020), https://doi.org/10.1016/J.NUCENGDES.2020.110767.

[7] D. Alfani, M. Astolfi, M. Binotti, P. Silva, Part-load strategy definition and preliminary annual simulation for small size sCO2-based pulverized coal power plant, J. Eng. Gas Turbines Power 143 (9) (2021), https://doi.org/10.1115/1.4051003/1108261.

[8] Z. Wang, J. Xu, T. Wang, Z. Miao, Q. Wang, G. Liu, Performance of sCO_2 coal-fired power plants at various power capacities, J. Clean. Prod. 416 (2023) 137949, https://doi.org/10.1016/J.JCLEPRO.2023.137949.

[9] F. Crespi, D. Sánchez, J.M. Rodríguez, G. Gavagnin, A thermo-economic methodology to select sCO_2 power cycles for CSP applications, Renew. Energy 147 (2020) 2905–2912, https://doi.org/10.1016/j.renene.2018.08.023.

[10] S.S.M. Shamsi, S. Barberis, S. Maccarini, A. Traverso, Large scale energy storage systems based on carbon dioxide thermal cycles: a critical review, Renew. Sust. Energ. Rev. 192 (2024) 114245, https://doi.org/10.1016/J.RSER.2023.114245.

[11] B. Lariviere, et al., sCO_2 power cycle development and STEP Demo pilot project, in: 4th sCO2 EU Conference, 2021, https://doi.org/10.17185/duepublico/73979.

[12] A. de la Calle, A. Bayon, Y.C. Soo Too, Impact of ambient temperature on supercritical CO_2 recompression Brayton cycle in arid locations: finding the optimal design conditions, Energy 153 (2018) 1016–1027, https://doi.org/10.1016/J.ENERGY.2018.04.019.

[13] P. Tafur-Escanta, I. López-Paniagua, J. Muñoz-Antón, Thermodynamics analysis of the supercritical CO_2 binary mixtures for Brayton power cycles, Energy 270 (2023), https://doi.org/10.1016/J.ENERGY.2023.126838.

[14] Scarabeus H2020 Project [Online]. Available, https://www.scarabeusproject.eu/, 2026.

[15] S.I. Salah, et al., Axial turbine flow path design for concentrated solar power plants operating with CO_2 blends, Appl. Therm. Eng. 230 (2023) 120612, https://doi.org/10.1016/J.APPLTHERMALENG.2023.120612.

[16] F. Crespi, et al., Thermal efficiency gains enabled by using CO_2 mixtures in supercritical power cycles, Energy 238 (2022), https://doi.org/10.1016/J.ENERGY.2021.121899.

[17] V.C. Illyés, G. Di Marcoberardino, A. Werner, M. Haider, G. Manzolini, Experimental evaluation of the CO_2-based mixture CO2/C6F6 in a recuperated transcritical cycle, Energy (2024) 133713, https://doi.org/10.1016/J.ENERGY.2024.133713.

[18] P. Rodríguez-deArriba, F. Crespi, D. Sánchez, A. Muñoz, T. Sánchez, The potential of transcritical cycles based on CO_2 mixtures: an exergy-based analysis, Renew. Energy 199 (2022) 1606–1628, https://doi.org/10.1016/J.RENENE.2022.09.041.

[19] G. Di Marcoberardino, et al., Experimental characterisation of CO2 + C6F6 mixture: thermal stability and vapour liquid equilibrium test for its application in transcritical power cycle, Appl. Therm. Eng. 212 (2022), https://doi.org/10.1016/J.APPLTHERMALENG.2022.118520.

[20] M. Doninelli, et al., Experimental investigation of the CO_2+$SiCl_4$ mixture as innovative working fluid for power cycles: bubble points and liquid density measurements, Energy 299 (2024) 131197, https://doi.org/10.1016/j.energy.2024.131197.

[21] P. Rodríguez-deArriba, F. Crespi, S. Pace, D. Sánchez, Mapping the techno-economic potential of next-generation CSP plants running on transcritical CO_2-based power cycles, Energy 310 (2024) 133142, https://doi.org/10.1016/J.ENERGY.2024.133142.

[22] Final report about most promising fluids with thermal stability and thermodynamic properties measurements - H2020 SCARABEUS PROJECT, Accessed: Jan. 23, 2026. [Online]. Available, https://cordis.europa.eu/project/id/814985/results, 2026.

[23] F. Crespi, P. Rodríguez de Arriba, D. Sánchez, A. Muñoz, Preliminary investigation on the adoption of CO_2-SO_2 working mixtures in a transcritical recompression cycle, Appl. Therm. Eng. 211 (2022), https://doi.org/10.1016/J.APPLTHERMALENG.2022.118384.

[24] E. Morosini, A. Ayub, G. di Marcoberardino, C.M. Invernizzi, P. Iora, G. Manzolini, Adoption of the CO_2 + SO_2 mixture as working fluid for transcritical cycles: a thermodynamic assessment with optimized equation of state, Energy Convers. Manag. 255 (2022), https://doi.org/10.1016/J.ENCONMAN.2022.115263.

[25] J. Xia, J. Wang, G. Zhang, J. Lou, P. Zhao, Y. Dai, Thermo-economic analysis and comparative study of transcritical power cycles using CO_2-based mixtures as working fluids, Appl. Therm. Eng. 144 (2018) 31–44, https://doi.org/10.1016/J.APPLTHERMALENG.2018.08.012.

[26] C. Wu, S. sen Wang, X. Jiang, J. Li, Thermodynamic analysis and performance optimization of transcritical power cycles using CO_2-based binary zeotropic mixtures as working fluids for geothermal power plants, Appl. Therm. Eng. 115 (2017) 292–304, https://doi.org/10.1016/J.APPLTHERMALENG.2016.12.077.

[27] J.Q. Guo, M.J. Li, J.L. Xu, J.J. Yan, K. Wang, Thermodynamic performance analysis of different supercritical Brayton cycles using CO_2-based binary mixtures in the molten salt solar power tower systems, Energy 173 (2019) 785–798, https://doi.org/10.1016/j.energy.2019.02.008.

[28] W.S. Jeong, J.I. Lee, Y.H. Jeong, Potential improvements of supercritical recompression CO_2 Brayton cycle by mixing other gases for power conversion system of a SFR, Nucl. Eng. Design 241 (6) (2011) 2128–2137, https://doi.org/10.1016/j.nucengdes.2011.03.043.

[29] J. Warren, G. Khawly, Commissioning and Operation of an Inventory Management System, 2024, https://doi.org/10.1115/GT2024-129457.

[30] X. Wang, et al., Dynamic simulation study of the start-up and shutdown processes for a recompression CO_2 Brayton cycle, Energy 259 (2022) 124928, https://doi.org/10.1016/J.ENERGY.2022.124928.

[31] M. Marchionni, M. Usman, L. Chai, S.A. Tassou, Inventory control assessment for small scale sCO_2 heat to power conversion systems, Energy 267 (2023) 126537, https://doi.org/10.1016/J.ENERGY.2022.126537.

[32] E. Morosini, et al., Preliminary characterization of the Desolination project demo plant: Design and off-design operability, in: ASME TURBOEXPO 2024, American Society of Mechanical Engineers Digital Collection, 2024, https://doi.org/10.1115/GT2024-127246.

[33] D. Alfani, M. Astolfi, M. Binotti, P. Silva, G. Persico, Part-load analysis and preliminary annual simulation of a constant inventory supercritical CO_2 power plant for waste heat recovery in cement industry, Energy 308 (2024) 132844, https://doi.org/10.1016/J.ENERGY.2024.132844.

[34] Baker Hughes - an energy technology company, Accessed (2026) [Online]. Available: https://www.bakerhughes.com/company/about-us.

[35] E. Morosini, et al., Off-design of a CO_2-based mixture transcritical cycle for CSP applications: analysis at part load and variable ambient temperature, Appl. Therm. Eng. 236 (2024) 121735, https://doi.org/10.1016/J.APPLTHERMALENG.2023.121735.

[36] B. Li, S. Wang, Y. Xu, L. Song, Study on the off-design performance of supercritical carbon dioxide power cycle for waste heat recovery of gas turbine, Energy Convers. Manag. 233 (2021) 113890, https://doi.org/10.1016/j.enconman.2021.113890.

[37] R.H. Ahmed, J. Al-Zaili, A.I. Sayma, Supercritical CO2 power cycle control strategies: a review, Appl. Therm. Eng. 280 (2025) 128135, https://doi.org/10.1016/j.applthermaleng.2025.128135.

[38] S. Sahai Gupta, P. Kumar, P.C. Gopi, Inventory management and control options for transient operation of sCO_2 Brayton cycles, J. Eng. Gas Turbines Power (2025) 1–51, https://doi.org/10.1115/1.4070112.

[39] Temisth SAS [Online]. Available, https://temisth.com/, 2026.

[40] V. Illyés, et al., Design of an Air-Cooled Condenser for CO2-Based Mixtures: Model Development, Validation and Heat Exchange Gain with Internal Microfins, in: Proceedings of ASME Turbo Expo 2022: Turbomachinery Technical Conference and Exposition 9, 2022, https://doi.org/10.1115/GT2022-82438.

[41] A. Cavallini, et al., Condensation in horizontal smooth tubes: a new heat transfer model for heat exchanger design, Heat Transfer Eng. 27 (8) (2006) 31–38, https://doi.org/10.1080/01457630600793970.

[42] Jonathan Wade, Prediction Methods of Settle Out Conditions and Design in sCO2 Power Cycles, Available: https://sco2symposium.com/proceedings2022/095-presentation.pdf, 2022.

[43] L.K. Dharmalingam, Review of Triply Periodic Minimal Surface (TPMS) Based Heat Exchanger Designs, International Refrigeration and Air Conditioning Conference, 2022.

[44] S.K. Mylavarapu, X. Sun, R.E. Glosup, R.N. Christensen, M.W. Patterson, Thermal hydraulic performance testing of printed circuit heat exchangers in a high-temperature helium test facility, Appl. Therm. Eng. 65 (1–2) (2014) 605–614, https://doi.org/10.1016/J.APPLTHERMALENG.2014.01.025.

[45] V. Gnielinski, New equations for heat and mass transfer in turbulent pipe and channel flow, Int. J. Chem. Eng. 16 (2) (1976) 359–368.

[46] A. Cavallini, D. Del Col, M. Matkovic, L. Rossetto, Frictional pressure drop during vapour–liquid flow in minichannels: modelling and experimental evaluation, Int. J. Heat Fluid Flow 30 (1) (2009) 131–139, https://doi.org/10.1016/J.IJHEATFLUIDFLOW.2008.09.003.

[47] E.D. Grimison, Correlation and utilization of new data on flow resistance and heat transfer for cross flow of gases over tube banks, J. Fluids Eng. 59 (7) (1937) 583–594, https://doi.org/10.1115/1.4020557.